Observation-based trends and drivers of global surface ocean acidification over the past four decades

Danling Ma[1], Luke Gregor[1], and Nicolas Gruber[2]

[1]ETH Zurich
[2]ETH Zürich

March 13, 2023

Abstract

The oceans are acidifying in response to the oceanic uptake of anthropogenic CO2 from the atmosphere, yet the global-scale progression of this acidification has been poorly documented so far by observations. Here, we fill this gap and use an observation-based product, OceanSODA-ETHZ, to determine the trends and drivers of the surface ocean aragonite saturation state (Ωar) and pH over the last four decades (1982-2021). In the global mean, Ωar and pH declined at rates of -0.071 ± 0.001 decade-1 and -0.0170 ± 0.0001 decade-1, respectively. These trends are driven primarily by the increase in the surface ocean concentration of dissolved inorganic carbon (DIC) in response to the uptake of anthropogenic CO2 but moderated by changes in natural DIC. Surface warming enhances the decrease in pH, accounting for 15% of the global trend. Substantial ENSO-driven interannual variability is superimposed on these trends, with Ωar showing greater variability than pH.

Observation-based trends and drivers of global surface ocean acidification over the past four decades

Danling Ma[1], Luke Gregor[1], and Nicolas Gruber[1]

[1]Environmental Physics, Institute of Biogeochemistry and Pollutant Dynamics, ETH Zurich, Zürich, Switzerland.

Key Points:

- From 1982 through 2021, surface ocean Ω_{ar} and pH declined at -0.071 ± 0.001 and -0.0170 ± 0.0001 per decade, respectively.
- These trends are predominantly caused by rising atmospheric CO2, with ocean warming enhancing the pH trend.
- ENSO dominates the interannual variability in Ω_{ar} and pH, although Ω_{ar} exhibits greater interannual variability.

Corresponding author: Nicolas Gruber, nicolas.gruber@env.ethz.ch

Abstract

The oceans are acidifying in response to the oceanic uptake of anthropogenic CO_2 from the atmosphere, yet the global-scale progression of this acidification has been poorly documented so far by observations. Here, we fill this gap and use an observation-based product, OceanSODA-ETHZ, to determine the trends and drivers of the surface ocean aragonite saturation state (Ω_{ar}) and pH over the last four decades (1982-2021). In the global mean, Ω_{ar} and pH declined at rates of -0.071 $\pm$ 0.001 decade^{-1} and -0.0170 $\pm$ 0.0001 decade^{-1}, respectively. These trends are driven primarily by the increase in the surface ocean concentration of dissolved inorganic carbon (DIC) in response to the uptake of anthropogenic CO_2, but moderated by changes in natural DIC. Surface warming enhances the decrease in pH, accounting for $\sim$ 15% of the global trend. Substantial ENSO-driven interannual variability is superimposed on these trends, with Ω_{ar} showing greater variability than pH.

Plain Language Summary

As the ocean takes up human-made CO_2 from the atmosphere, it becomes more acidic, i.e., its pH is dropping and so is its saturation state (Ω_{ar}) with respect to aragonite, a type of carbonate mineral. These chemical changes, generally referred to as "Ocean Acidification", are harming marine organisms. Here, we use an observation-based data set to investigate the trends and drivers of these two important metrics of acidification in global surface ocean over the last four decades (1982-2021). Our results confirm that pH and Ω_{ar} have been declining across the global ocean during the study period and that these trends are predominantly driven by the increase in the surface ocean concentration of dissolved inorganic carbon resulting from the accumulation of human-made CO_2. We also show that the observed ocean warming enhances the decline in pH. Both metrics, and especially Ω_{ar} vary substantially around these long-term trends, largely in response to El Niño events in the tropics. Our study provides, for the first time, a global observation-based quantification of the progression and driving factors of ocean acidification, which will help to better understand the impact of ocean acidification on marine life.

1 Introduction

The oceans provide a large ecosystem service by taking up roughly a third of the CO_2 emitted by anthropogenic activities (Friedlingstein et al., 2022; Sabine et al., 2004; Khatiwala et al., 2013; Gruber et al., 2023), but this comes at a substantial cost, i.e., ocean acidification (OA) (Caldeira & Wickett, 2003; Orr et al., 2005; Doney et al., 2009). While the term acidification stems from the fact that CO_2 taken up from the atmosphere and added to seawater liberates protons, i.e., increases the concentration of H^+ and thus lowers seawater pH (pH = -log [H^+]), OA refers to a larger set of chemical changes in seawater. Some of the CO_2 that is taken up is titrated away by carbonate ions dissolved in seawater (Sarmiento & Gruber, 2006), reducing the concentration of these ions. This causes the saturation state of calcium carbonate $CaCO_3$ minerals (Ω), such as that of aragonite (Ω_{ar}), to decline.

Ocean acidification has been the subject of much research in the past two decades since it can severely impact marine life (R. A. Feely et al., 2004; Orr et al., 2005; Doney et al., 2009; Gruber et al., 2012; Jiang et al., 2019; Kroeker et al., 2013). This impact can occur at the level of an individual organism by affecting, e.g., its physiology or behavioral patterns (Doney et al., 2020; Figuerola et al., 2021; Radford et al., 2021; Cornwall et al., 2022). It can also occur all the way up at the scales of communities and ecosystems, e.g., by altering population dynamics or by knocking out keystone species and thereby altering community structure (Hall-Spencer & Harvey, 2019; Doney et al., 2020; Corn-

wall et al., 2021; Harvey et al., 2021). Thus, it is critical that we understand the historical progression and contemporary state of OA across the global ocean. This would permit us also to make better predictions of what the future may hold. However, the ability of the oceanographic community to quantitatively describe the past progression of OA across the global ocean with observations has been remarkably limited. This contrasts with model-based studies which clearly established past and future trends of OA (Orr et al., 2005; R. A. Feely et al., 2009; Friedrich et al., 2012; Bopp et al., 2013; Kwiatkowski et al., 2020; Terhaar et al., 2023).

This lack of observation-based studies of OA trends is in part due to the limited number of historical observations available for the key parameters of OA, i.e., $[H^+]$, pH, and Ω_{ar}. For example, seawater pH measurements before 1989 relied primarily on glass electrodes, which involve uncertainties of the order of 0.1 pH units. This is too uncertain to capture the pH alterations induced by OA, rendering these observations unusable. A further complication arises because the pH scale of many earlier records is ambiguous (Jiang et al., 2019). The availability and quality of seawater pH data has improved gradually in the subsequent decades, following the refinement of spectrophotometric pH measurement methods (Byrne & Breland, 1989; Clayton & Byrne, 1993; A. G. Dickson, 1993; Jiang et al., 2019). These developments have been greatly aided by efforts such as the Global Ocean Acidification Observing Network (GOA-ON) (Brewer, 2013; Tilbrook et al., 2019), which supported communities around the world to make high quality measurements, especially in coastal regions. Also, the recent advent of the biogeochemical Argo program with pH sensors has dramatically increased the amount of available data in the last few years, especially in the open seas (Claustre et al., 2020). But the temporal coverage of these data is very limited, preventing an assessment of OA changes over multiple decades. For the saturation state Ω_{ar} or the concentration of the carbonate ion in seawater, the situation is even worse, as they are typically not measured directly. This leaves no record from which changes in time can be deduced directly.

For these reasons, observation-based OA trend studies have used pH, $[H^+]$, and Ω_{ar} computed from the more frequently measured variables of the ocean carbonate system, namely the partial pressure of CO_2 (pCO_2) and total alkalinity (Alk) (Bates, 2007; Bates et al., 2014; Lauvset & Gruber, 2014; Lauvset et al., 2015; Jiang et al., 2019). Most studies so far have applied this approach for local to regional studies, relying primarily on the data from the few existing long-term time series sites (Bates, 2007; Bates et al., 2014; Olafsson et al., 2010) or the few regions where sufficient observations exist to establish trends directly (Sutton et al., 2014; Kim et al., 2014; Leseurre et al., 2022). These studies unequivocally demonstrated that the ocean is acidifying, revealing highly significant long-term decreases in pH and Ω_{ar} at all sites and regions. But the community lacks an observation-based global-scale analysis that permits researchers to put these local and regional trends into context and also allows them to assess regional differences.

A first attempt to establish global trends in OA based solely on observations was made by Lauvset et al. (2015) who used measured pCO_2 and empirical estimates of Alk to estimate trends in surface ocean pH. They found significant pH decreases in ∼70% of all large-scale biomes and a mean rate of decrease of 0.018 ± 0.004 decade^{-1} for 1991–2011. But their study did not include Ω_{ar}, had insufficient data in several key regions such as the Southern Ocean, required a large amount of spatial aggregation leading to a very low resolution, and was limited in time to two decades. Building on this work and its own synthesis of the data from various time series sites across the world's oceans, the Intergovernmental Panel on Climate Change (IPCC) concluded in its special report on the Ocean and Cryosphere (Bindoff et al., 2019), that "pH in open ocean surface water has changed by a virtually certain range of –0.017 to –0.027 pH units per decade since the late 1980s." IPCC's Working Group 1 report in AR6 confirmed in essence this very large range for the global mean rate, and also discussed the spatial variability around this mean trend (Canadell et al., 2021). An alternative approach was taken more recently

by Jiang et al. (2019) who combined a climatological seawater CO_2 product with model results to obtain trends in the OA parameters. But by relying on a model for establishing the trends, this estimate cannot really be considered observation-based. Thus, while there is a pressing need for an observation-based assessment of the trends and drivers of OA on a global scale, the existing analyses are insufficient to fulfil this need. This gap is even more evident when compared to the huge volume of literature on long-term trends and variability in surface ocean pCO_2 (A. Fay & McKinley, 2013; Tjiputra et al., 2014; Landschützer et al., 2014; Rödenbeck et al., 2015; Landschützer et al., 2016; A. R. Fay et al., 2021; Gloege et al., 2022).

To close this gap, we present a global-scale analysis on the trends and drivers in both surface ocean pH and Ω_{ar} using an updated version of the OceanSODA-ETHZ observation-based product (Gregor & Gruber, 2021). This updated product covers the period from 1982 to 2021 at a spatial resolution of $1° \times 1°$, and at monthly resolution in time, and thus provides not only much higher resolution than the previous analysis by Lauvset et al. (2015), but also doubles the length of the analyzed time period. OceanSODA-ETHZ was derived by combining in-situ observations of pCO_2 and Alk with a range of satellite observations using a machine-learning approach. In this product, the surface ocean $[H^+]$, pH and Ω_{ar} are computed from the mapped pCO_2 and Alk data. Since this approach explicitly also involves the determination of the concentration of dissolved inorganic carbon (DIC), it permits us to analyze also the main drivers for the changes in $[H^+]$, pH and Ω_{ar}.

2 Materials and Methods

2.1 OceanSODA-ETHZ dataset and trend analyses

We use the global surface $[H^+]$, pH, and Ω_{ar} data from OceanSODA-ETHZ to analyze long-term trends in global OA from 1982 through 2021 (Gregor & Gruber, 2021). OceanSODA-ETHZ is an observation-based, global gridded data set with monthly data for ocean carbonate system parameters at a resolution of $1° \times 1°$. It was derived with a two-step machine learning approach (clustering and regression) that maps the observed distribution of pCO_2 and Alk to the global ocean using a range of independent variables as predictors. The version used here was updated from the published version by including data for the years 2020 and 2021. The OceanSODA-ETHZ product computed $[H^+]$, pH, Ω_{ar} and DIC from the mapped pCO_2 and Alk distribution by solving the marine carbonate system:

$$\Omega_{ar}, \mathrm{pH}, [H^+], DIC, \ldots = \mathrm{PyCO2SYS}(p\mathrm{CO}_2, Alk, T, S, Nutrients) \quad (1)$$

where PyCO2SYS is the software used to solve the marine carbonate system (Humphreys et al., 2020). For the dissociation constants of the marine carbonate system, we used the Mehrbach et al. (1973) constants refitted by A. Dickson and Millero (1987), as this gives the lowest uncertainty whenpCO_2 and Alk are used as input (Raimondi et al., 2019). Additional inputs consist of sea-surface temperature (T), sea-surface salinity (S), and the concentrations of the nutrients silicate and phosphate. Sea-surface temperature was taken from the NOAA OI SST V2 High-Resolution Dataset (OISSTv2; Reynolds et al., 2007), while sea-surface salinity is a combination of the ESA-CCI sea surface salinity product for 2010 to 2020 (Boutin et al., 2018) and Simple Ocean Data Assimilation (SODA v3.4.2; Carton et al., 2018) where the ESA-CCI product is not available. Silicate and phosphate concentrations were taken from the World Ocean Atlas 2018 (Boyer et al., 2018).

Following many previous studies (e.g., Lauvset et al., 2015; Bates et al., 2014), we use here the total scale for pH, which includes the contribution of sulfate ions (A. G. Dickson, 1993). In contrast, we report for $[H^+]$ its free concentration, which is equivalent to pH on the free scale (Clayton & Byrne, 1993), i.e., without the contribution of the sul-

fate ions. We use the saturation state of Ω_{ar} as the second metric to quantify the evolution of OA (Mucci et al., 1983; Takahashi et al., 2014). Although aragonite is ∼50% more soluble than calcite, the trends for its two saturation states tend to be nearly identical.

Trends are calculated on annual averages using an ordinary least squares (OLS) regression. We thereby determined the uncertainties of the trends based on the two-sided inverse Students t-distribution for a 95% confidence interval with $(n-2)$ degree of freedom, where n is the number of data in the global mean time series. The uncertainties of the global mean trends are then computed by multiplying the critical value of the t-distribution with the standard errors of the estimate for the slopes. The reported uncertainty thus reflects only the uncertainty of the trend and thus does not include any error in the underlying data.

2.2 Driver decomposition of trends

We decompose the trends in Ω_{ar} and $[H^+]$ into contributions from trends in the main drivers, that is DIC, Alk, T and freshwater (FW). The freshwater driver includes both the direct effect of changes in salinity on Ω_{ar} and pH, as well as the indirect effect caused by changes in the surface ocean DIC and Alk due to the net freshwater balance (Lovenduski et al., 2007; Landschützer et al., 2018). To this end, we remove the freshwater component from the DIC and Alk driver by normalizing these two parameters to a constant salinity of 34.5 (Sarmiento & Gruber, 2006; Landschützer et al., 2018). The resulting quantities are denoted by sDIC and sAlk. We further decompose DIC into an anthropogenic and a natural component, DIC = $C_{ant} + C_{nat}$, i.e., the component driven solely by the anthropogenic increase in atmospheric CO_2 and the resulting uptake of anthropogenic CO_2 by the surface ocean, and the component driven by changes in circulation and biology (McNeil & Matear, 2013; Gruber et al., 2023).

Neglecting the contributions from other minor drivers such as nutrients, we thus decompose the variations in the trends of Ω_{ar} and $[H^+]$ to five main driving components: anthropogenic sDIC (C_{ant}), natural sDIC (C_{nat}), sAlk (A), temperature (T) and freshwater (FW). Considering only the first-order terms of a Taylor expansion and using the product rule, this gives the rate of change of Ω_{ar}:

$$\frac{d\Omega_{ar}}{dt} = \sum_{X=[C_{ant},C_{nat},A,T,FW]} \left(\underbrace{\frac{d\omega_X}{dt} \cdot \Omega_{ar} \cdot \Delta X}_{\text{change in sensitivity}} + \underbrace{\omega_X \cdot \frac{d\Omega_{ar}}{dt} \cdot \Delta X}_{\text{mass effect}} + \underbrace{\omega_X \cdot \Omega_{ar} \cdot \frac{d\Delta X}{dt}}_{\text{change in driver}} \right), \tag{2}$$

where X is one of the five drivers, ΔX is the change in the driver (from 1982 through 2021), and ω_X is the relative sensitivity of Ω_{ar} to each driver, i.e., $\omega_X = 1/\Omega_{ar} \cdot \partial\Omega_{ar}/\partial X$. Note that this definition of ω_X differs from that of Egleston et al. (2010) who defined it as the sensitivity of X to Ω_{ar}. The time derivatives on the right-hand side of (2) are determined from the slopes of the linear regressions.

The same decomposition is applied for $[H^+]$, i.e.,

$$\frac{d[H^+]}{dt} = \sum_{X=[C_{ant},C_{nat},A,T,FW]} \left(\underbrace{\frac{d\beta_X}{dt} \cdot [H^+] \cdot \Delta X}_{\text{change in sensitivity}} + \underbrace{\omega_X \cdot \frac{d[H^+]}{dt} \cdot \Delta X}_{\text{mass effect}} + \underbrace{\omega_X \cdot [H^+] \cdot \frac{d\Delta X}{dt}}_{\text{change in driver}} \right), \tag{3}$$

where β_X is the relative sensitivity of [H$^+$] to each driver X, i.e., $\beta_X = 1/[H^+] \cdot \partial[H^+]/\partial X$. The relative sensitivities β and ω are calculated with the PyCO2SYS program (Lewis et al., 1998; Humphreys et al., 2020) for each grid point, using the long-term average conditions as input. The temperature sensitivities are assumed to be constant for the entire range of DIC and Alk, with a value of 0.0052 °C^{-1} for Ω_{ar} and a value of 0.0354 °C^{-1} for [H$^+$].

The surface ocean concentration of C_{ant} and its rate of change is estimated by assuming that surface ocean DIC increases proportionally with the increase in atmospheric CO_2 (Gruber et al., 2023). We determine this proportionality by computing first the amount of C_{ant} the surface ocean would have if it had remained in transient equilibrium with the overlying atmosphere, i.e., the C_{ant}^{eq} component. We then adjust this component to account for the fact that the increase in surface C_{ant} is increasingly delayed, leading to a growing disequilibrium term, i.e., C_{ant}^{dis-eq}, which is also proportional to the rise in atmospheric CO_2 (see Matsumoto and Gruber (2005) for a more in-depth discussion). Concretely, C_{ant} is given by: $C_{ant} = C_{ant}^{eq}$ - C_{ant}^{dis-eq}. We determine C_{ant}^{eq} at each surface location by evaluating (1) whereby the in situ pCO_2 is replaced with atmospheric CO_2 from the NOAA marine boundary layer product (Dlugokencky et al., 2021). We take the disequilibrium term C_{ant}^{dis-eq} from a hindcast simulation with the ocean component of the Community Earth System Model (CESM) (Clement & Gruber, 2018; Hauck et al., 2020). The trend in the natural component, C_{nat}, is computed by subtracting C_{ant} from sDIC, i.e., C_{nat} = sDIC - C_{ant}, whereby all components are salinity normalised to 34.5.

2.3 Time of Emergence

The Time of emergence (ToE) is defined as the time it takes for a signal to arise from the noise of natural climate variability (Keller et al., 2014):

$$\text{ToE} = (2 \times \text{N})/\text{S} \tag{4}$$

where N is the standard deviation of the detrended and deseasonalized monthly data, and S is the annual trend. This results in TOE having an output in units of years.

3 Results and Discussions

3.1 Evaluation

The rate of pH change estimated from OceanSODA-ETHZ generally agrees well with the reported rates from observation stations around the globe (Table S1 in the supplementary material). However, many stations have reported trends over much shorter periods, making the comparisons less robust owing to a stronger imprint of interannual variability. We thus focus the evaluation of our trend estimates with those stemming from the longest-running (> 30 years) and best-sampled time series sites in the ocean, namely the Hawaii Ocean Time-series (HOT) (Dore et al., 2009) in the North Pacific, the Bermuda Atlantic Time series Study (BATS) in the North Atlantic (Bates et al., 2014; Bates & Johnson, 2020) (Table S2). This evaluation is particularly insightful since the data from these two time series sites were not used for the training of the machine-learning algorithm in OceanSODA-ETHZ. Neither site measured pH or Ω_{ar}, but DIC and Alk, from which we computed pH and Ω_{ar} following the same procedures as for OceanSODA-ETHZ. We also recomputed the long-term trends in order to ensure maximum comparability with our estimates. To this end, we first deseasonalized the data from the time series stations using a harmonic fit (Gruber et al., 2002) and then computed the trend in the same manner as done for OceanSODA-ETHZ.

For BATS and the period covered by this site, i.e., 1992-2021, we compute for OceanSODA-ETHZ a decadal rate of change for pH of -0.017±0.001 decade^{-1}, numerically identical to what we determined from the reported time series data. By including data from the

nearby Station "S" (Gruber et al., 2002), Bates and Johnson (2020) was able to extend this record back in time, reporting for 1983-2020 a slightly more negative trend of -0.019±0.001 decade^{-1} (Table S1), a bit more negative than our estimate for the same period (-0.016±0.001), but still within the uncertainties. The trends for Ω_{ar} are slightly more different, but still in agreement. While our estimate for the period 1992-2021 of -0.061±0.005 decade^{-1} is again numerically identical to that we computed from the time series data, Bates and Johnson (2020) found for the combined Station "S" and BATS sites over the 1983-2020 period a trend of -0.09±0.01 decade^{-1}, which is quite a bit more negative than ours (Table S1).

Our pH trend estimate for the HOT site (1989-2021) of -0.018±0.001 decade^{-1} is again the same as that we computed from the reported time series data (-0.018±0.001 decade^{-1}). But, as was the case at BATS, there is a somewhat less agreement on the trend in Ω_{ar}. For OceanSODA-ETHZ, we find a trend of -0.083±0.005 decade^{-1}, while for the time series data, the trend amounts to -0.089±0.006 decade^{-1}.

The evaluation of the trends at the other time series sites (Table S1 in the supplementary material), often of much shorter duration, confirms the overall excellent agreement. But this comparison also suggests that the OceanSODA-ETHZ has a slight tendency for underestimating long-term trends, especially for Ω_{ar}. This could be a consequence of the cluster-regression approach that we employed in ensemble mode to create OceanSODA-ETHZ, as this machine-learning method tends to suppress variations and trends (Gregor & Gruber, 2021). Still, these evaluations suggest that OceanSODA-ETHZ reproduces the observed long-term trends at the time series stations with high fidelity, giving us confidence in the use of this product to assess long-term trends in OA across the global ocean (Chau et al., 2022).

3.2 Long-term trends

The temporal evolution of the reconstructed global surface mean Ω_{ar}, pH, and $[H^+]$ from the OceanSODA-ETHZ product confirm the expected strong trends induced by ocean acidification over the four decades from 1982 through 2021 (Fig. 1). Averaged over the global ice-free ocean, surface Ω_{ar} decreased by nearly 10% over these four decades, and pH experienced a drop of ∼0.06 units. At the same time, $[H^+]$ increased proportionately by slightly more than 1 nmol kg^{-1}. This translates into highly significant average trends of -0.071 ± 0.001 decade^{-1} for Ω_{ar} ($R^2 = 0.98$; $p \ll 0.01$) and -0.0170 ± 0.0001 decade^{-1} for pH ($R^2 = 0.99$; $p \ll 0.01$). For $[H^+]$ the average rate of increase amounts to 0.240 ± 0.004 nmol kg^{-1} decade^{-1}. The global trends are very insensitive to the choice of the exact beginning or ending years. For example, shortening the record to 30 years and computing the trends by shifting the beginning year from 1982 to 1992 yields variations in the trends of $< 7\%$.

The reported uncertainties of the trends reflect just the statistical uncertainty of the regression slope, and thus do not include any additional uncertainties induced by systematic errors associated with the underlying data. In order to obtain a zeroth order estimate of this contribution, we determined the trends for each individual ensemble member in the OceanSODA-ETHZ product and computed the resulting standard deviation. This resulted in essentially the same uncertainty as the reported trend uncertainty. Larger contributions to the trend uncertainty could stem from biases in our mapped product that change with time, such as those that could be induced from changed sampling through time, or from temporally changing systematic errors in the measurements of pCO_2 and/or alkalinity that underlie the OceanSODA-ETHZ product. Although we have not found any indication of such temporally changing errors (Gregor & Gruber, 2021), we cannot exclude this either. We thus conclude that the reported trend uncertainties are likely an underestimate, perhaps by several fold. Even if we adopted, for example, a fivefold increase in the uncertainty, the relative uncertainties of the trend estimates would remain

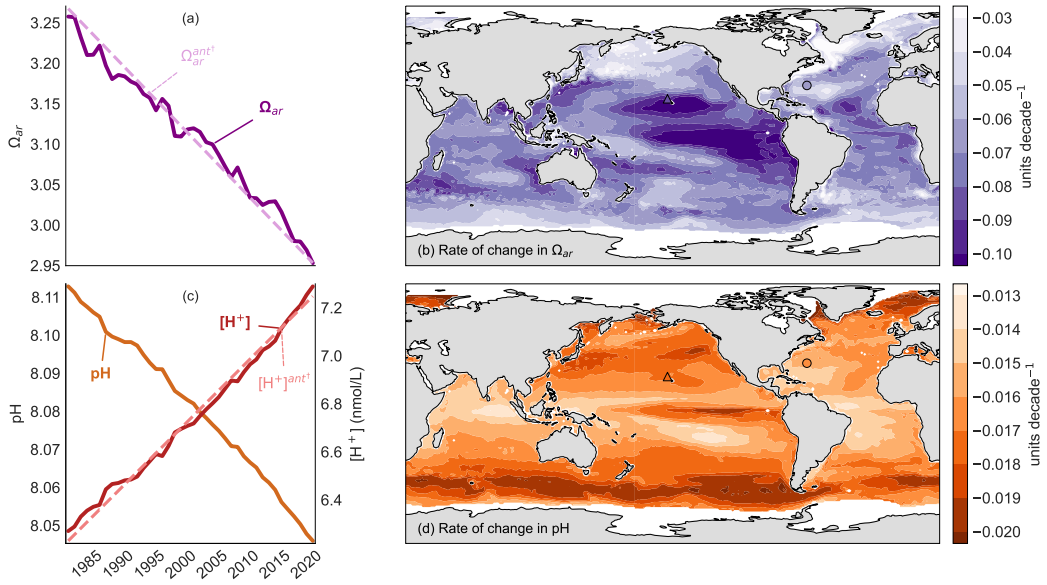

Figure 1. Temporal and spatial structure of the long-term trends in global aragonite saturation state (Ω_{ar}), pH, and [H^+] from 1982 to 2021 using OceanSODA-ETHZ data (Gregor & Gruber, 2021). (a) Global area-weighted trend for Ω_{ar} (solid line), along with the estimated anthropogenic trend (dashed line) based on the increase in C_{ant}. (b) Global map of the 40-year average trend of Ω_{ar}, expressed as trend per decade. (c) As (a) but for pH (left axis) and [H^+] (right axis) with the estimated anthropogenic increase being shown for the latter only. (d) As (b), but for pH. Note that the global average trends plotted in (a) and (c) are computed over the colored areas shown in (b) and (d), representing 96% of the global sea-ice-free surface area. The triangle and circle in (b) and (d) indicate the locations of the two time series HOT and BATS used to evaluate the OceanSODA-ETHZ product in detail.

at less than 10%. We consider this an extremely pessimistic case, but we lack information to provide a better estimate of the true uncertainty.

Our global mean surface pH trend supports the trend estimated by Lauvset et al. (2015) of 0.018±0.004 for the period 1991 through 2011, we can now provide a much more accurate estimate covering 96% of the global sea-ice-free surface ocean as opposed to the 70% coverage available to Lauvset et al. (2015). Even when considering our potential underestimation of the trend uncertainty, our estimate permits us also to reduce the range given by IPCC (Bindoff et al., 2019), i.e., -0.017 to -0.027 decade^{-1}, by more than tenfold. Our global pH trend matches also well those given by a range of Earth System Models (Kwiatkowski et al., 2020). Unfortunately, we are unaware of reported global ocean mean trends for Ω_{ar}.

Spatially, the rates of the Ω_{ar} and pH declines over the past four decades vary substantially across the open ocean (Fig. 1b,d)(see also Suppl. Tables S3 and S4). For Ω_{ar}, the largest trends are found in the tropical and subtropical Pacific Ocean, including the eastern tropical Pacific region (Fig. 1b), with rates of Ω_{ar} decreases that are, on average, 50% higher than in the global mean. In contrast, Ω_{ar} drops much less in the North Pacific and North Atlantic and parts of the Southern Ocean. Here, rates tend to be only half those of the global mean. This gives overall a factor of four difference in rates across the global ocean, highlighting the importance of the regional perspective when investigating ocean acidification.

The spatial distribution of the decline in pH tends to be the mirror image of that of Ω_{ar} (Fig. 1d), although the range is smaller. The highest rates of decline are found in the Southern Ocean and in the high latitudes of the North Atlantic and North Pacific. Rates are here, expressed in the logarithmic pH units, about 15% higher than in the global mean. The lowest rates of changes are found in the subtropical gyres, with rates that are about 25% lower than the global mean. Another striking pattern is that the trends in the Pacific tend to be larger than those in the Pacific for the same latitude. A region that breaks the mirror image, i.e., where both Ω_{ar} and pH show large changes, is a small equatorial band in the eastern and central Pacific.

The distinct spatial variations of the rates of change of ocean acidification had been discussed in the literature only sparingly so far. Lauvset et al. (2015) also found trends that varied considerably across the analyzed biomes, but given the large uncertainties of their regional trends, they refrained from discussing them in detail. They did point to the systematic differences between the Atlantic and Pacific, however. A systematic difference we can confirm here. In its global assessment, IPCC AR6 (Canadell et al., 2021) discussed the regional differences as well, pointing out, for example, that the central and eastern upwelling zones of the Pacific exhibited a faster pH decline of –0.022 to –0.026 decade^{-1} (see also Sutton et al. (2014)) compared to the western tropical Pacific, where the trends are only in the range of –0.010 to –0.013 decade^{-1} (see also Ishii et al. (2020)). This strong east-west gradient in the tropical Pacific is fully confirmed by our results (Fig. 1d). IPCC AR6 further suggested for the subtropical gyres pH trends ranging from -0.016 to -0.019 decade^{-1}, which is a smaller range than that we find (-0.013 to -0.019 decade^{-1}). In contrast, IPCC AR6 suggests subpolar latitudes values ranging from -0.003 decade^{-1} to -0.026 decade^{-1}, while our work suggests a substantially smaller range (-0.017 to -0.020 decade^{-1}). We interpret these differences to be primarily the result of the relatively small number of time series sites that were used by the IPCC for their assessment. We are not aware of any study that investigated the spatial pattern of the trend in Ω_{ar} in a systematic manner, although IPCC AR6 (Canadell et al., 2021) mentioned the regional differences.

3.3 Drivers of the long-term trends

The driver decomposition (2) & (3) confirms the expectation that the majority of the decreasing trend in Ω_{ar} and increasing trend in $[H^+]$ is driven by the anthropogenic increase in atmospheric pCO_2 causing an increase in surface ocean C_{ant} (dashed lines in Fig. 1a,c). This conclusion is in line with IPCC's assessments (Canadell et al., 2021; Bindoff et al., 2019) as well as with prior work (Lauvset & Gruber, 2014; Lauvset et al., 2015). However, hidden behind the dominating role of C_{ant} are substantial and relevant contributions from the other drivers. A first indication of this comes from the global trend in Ω_{ar} in Fig. 1a), which is decreasing substantially less rapidly than expected from the anthropogenic trend alone. This differs markedly from the trends in pH and $[H^+]$, which agree remarkably well with the anthropogenic trend. A second indication comes from the full driver decomposition in Fig. 2a,b, which show that changes in natural CO_2, temperature, and to a somewhat smaller degree also sAlk, contribute substantially to the trends, especially for $[H^+]$. We discuss these two indications in sequence.

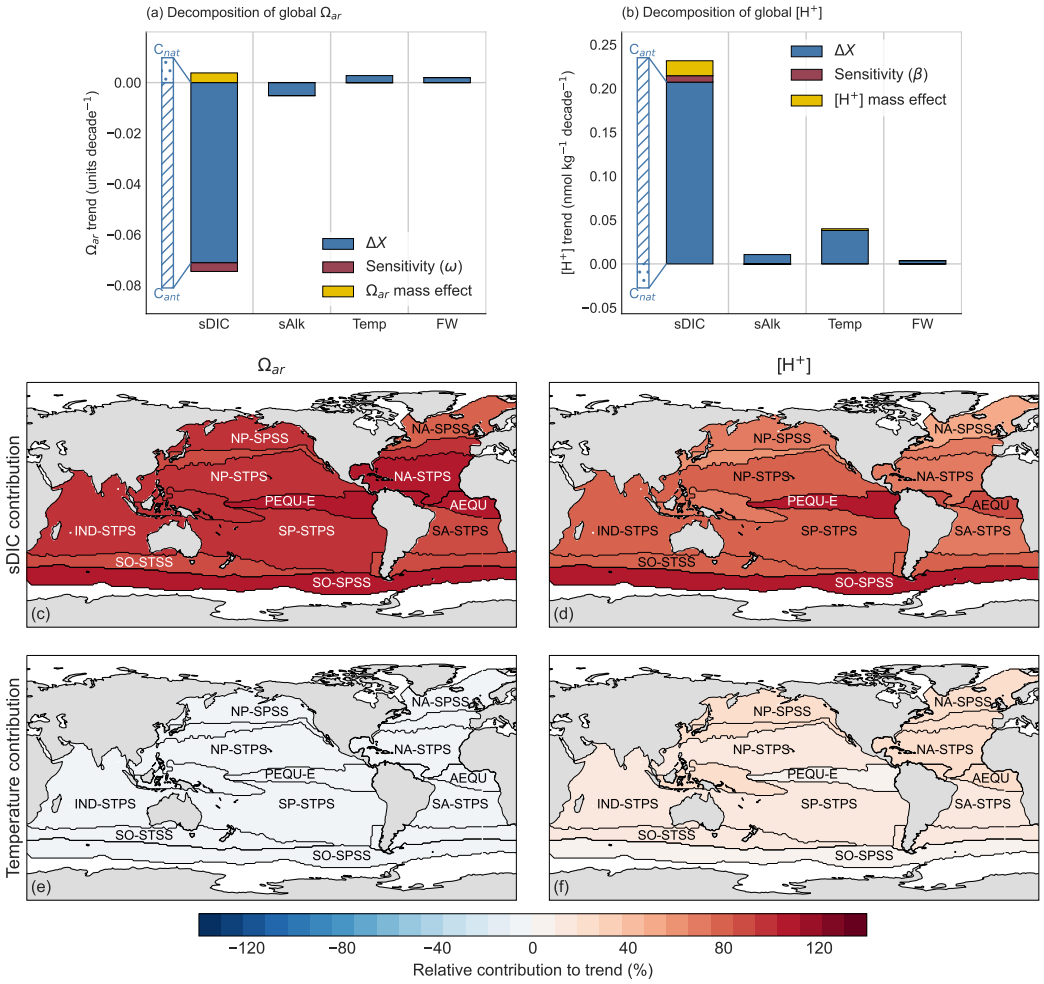

Figure 2. Decomposition of the global mean rate of change of (a) Ω_{ar} and (b) [H$^+$] over the period 1982-2021 into their main drivers following equations (2) & (3) in the main text. The considered drivers are: salinity normalized dissolved inorganic carbon (sDIC) separated into its anthropogenic CO2 (C_{ant}) and natural CO2 (C_{nat}) components, sea surface temperature (SST), salinity normalized alkalinity (sAlk), and freshwater (FW). Also shown for each driver are the contribution of the three mechanisms: change in the driver sensitivity (blue), change in the carbonate system variable (yellow), and change in the driver itself (red). Also shown here are maps showing the relative contribution of (c) sDIC to the rate of change of Ω_{ar}, (d) sDIC to the trend of $[H^+]$, (e) SST to the trend in Ω_{ar}, and (f) SST to the trend in $[H^+]$ aggregated to each biome.

According to our decomposition, the main reason for the smaller than expected long-term trend in Ω_{ar} is the substantial compensation by natural CO2 (C_{nat}) (Fig. 2a). This means that in the OceanSODA-ETHZ product, the concentration of sDIC is not increasing as fast as predicted from the increase in anthropogenic CO2 (C_{ant}) because of a loss in C_{nat}. Since changes in sAlk are relatively minor and even suggesting a small increase, this smaller than expected increase in sDIC causes a lower rate of decrease of the carbonate ion concentration predicted from the increase in C_{ant} alone, hence causing a lower rate of decrease of Ω_{ar}. Also warming and the freshwater component actually act to compensate for the anthropogenic CO2 driven decrease in Ω_{ar}, but their contribution is small (Fig. 2a). Similarly, the mass effect slows the rate of decrease of Ω_{ar}. In summary, the

contribution of the non-sDIC components is small, so that it is the decrease in C_{nat}, i.e., the reduction in the concentration of natural CO_2 in the surface ocean, that causes global mean Ω_{ar} to decrease less rapidly than predicted from the rise in atmospheric CO_2 alone.

The decomposition of the trends for $[H^+]$ reveals a different picture (Fig. 2b). While the strong increase in $[H^+]$ driven by C_{ant} is also compensated by the decrease in C_{nat}, the other components, are contributing substantially to the driving up of the trend in $[H^+]$ (Fig. 2b). The most important driver is temperature, which contributes $\sim$ 15% to the rate of increase in $[H^+]$. But also the $[H^+]$ mass effect and the increased sensitivity contribute to the rise in $[H^+]$. Taken together, a different balance emerges for the trend in $[H^+]$ compared to that of Ω_{ar}. For $[H^+]$, the slowing trend induced by the loss of C_{nat} is nearly entirely compensated for by the accelerating trend induced by surface ocean warming, so that the overall trend is remarkably close to that predicted by C_{ant} alone. In other words, the loss of C_{nat} tends to mask the quite substantial accelerating contribution of ocean warming on the trend of $[H^+]$.

Thus for both trends, we find an important modification of the purely anthropogenic CO_2 trend by surface ocean warming and the loss of C_{nat}, albeit with different relative roles. Before we discuss this finding further, we need to ensure that it is robust. This is especially critical since we estimate the trend in C_{nat} by difference from the trend in sDIC and C_{ant}. Of particular concern is our estimate of the disequilibrium component, which we use to adjust the equilibrium estimate of C_{ant} for the fact that even in the absence of any climate variability surface ocean sDIC is not following perfectly the increase in atmospheric CO_2 owing to the slowness of air-sea gas exchange and limited surface residence times (Matsumoto & Gruber, 2005). Globally, the mean air-sea disequilibrium is actually very well-constrained since it is directly related to the oceanic uptake of anthropogenic CO_2, which is known to within about $\pm$15% on the basis of multiple approaches (Gruber et al., 2023, 2019; Hauck et al., 2020; DeVries, 2014; Mikaloff Fletcher et al., 2006; Sabine et al., 2004). It turns out that even adopting an uncertainty for the air-sea disequilibrium of C_{ant} of $\pm$30% would not alter our conclusion that C_{nat} has decreased over the last four decades. We thus consider this conclusion as robust.

The diagnosed loss of C_{nat} from the surface ocean slowing down the rate of change of Ω_{ar} and $[H^+]$ can also be rationalized from a process perspective, especially since it is connected to surface ocean warming. First, one expects a loss of C_{nat} form the surface ocean in response to the reduced CO_2 solubility associated with surface warming (Weiss, 1974). Second, upper ocean warming has been linked to the observed increase in upper ocean stratification (Sallée et al., 2021), which tends to make the biological pump more efficient, causing a reduction in surface ocean DIC (Sarmiento & Gruber, 2006).

The important contribution of ocean warming to the long-term trend in $[H^+]$ becomes also very clear when investigating this decomposition on a regional basis, here shown just for the contribution from sDIC, i.e., the sum of natural and anthropogenic CO_2 (Fig. 2c-d), and for temperature (Fig. 2e-f). While the contribution of warming to the trend in Ω_{ar} is less than a few percent, this number is about 8% for $[H^+]$, on average. The highest contributions are found in the North Atlantic and the western Pacific, i.e., the regions that experienced the highest rates of surface warming in the last few decades (Johnson & Lyman, 2020).

Still, the majority of the long-term trend for both $[H^+]$ and Ω_{ar} across all regions stem from the increase in sDIC (Fig 2c-d). This means that the distinct spatial differences in the rates of change in $[H^+]$ and Ω_{ar} seen in Fig. 1 and shown as zonal means in Fig 3.3c,f are caused by the product of the spatial pattern of the sensitivities β_{DIC} and ω_{DIC}, respectively with the trend in C_{ant} (see Fig. supplementary S5), whose spatial pattern is given by the inverse of the sensitivity γ_{DIC} (Egleston et al., 2010). This means that one can understand the trends in $[H^+]$ and Ω_{ar} as being proportional to the ratio of β_{DIC}/γ_{DIC} and $\omega_{DIC}/\gamma_{DIC}$, respectively (see also Orr (2011) for a detailed dis-

cussion). All of these sensitivities are reflections of how well the surface carbonate chemistry is able to buffer the increase in surface ocean CO_2, which depends on temperature, and especially the ratio of DIC and Alk (Sarmiento & Gruber, 2006; Egleston et al., 2010).

In the case of the trends in $[H^+]$ (and pH), the high sensitivity of β_{DIC} at the high latitudes (Figure S4), largely driven by temperature, overwhelms the impact of the higher rates of change in C_{ant} in the low latitudes owing to higher buffer capacities (Sabine et al., 2004) (or lower γ_{DIC}), such that the highest rates of changes in $[H^+]$ (pH) are found in the high latitudes. For Ω_{ar}, the situation is reversed. Here the high buffer capacity of the low latitudes (small γ_{DIC}) with the corresponding higher rates of accumulation of C_{ant} overwhelms the effect of ω_{DIC}, which has the highest (absolute) sensitivity in the high latitudes as well. The net result is that the highest rates of change in Ω_{ar} occur in the low latitudes. This also means that the highest decreases in Ω_{ar} occur in the regions where Ω_{ar} is highest, while for $[H^+]$, the highest increases occur where $[H^+]$ is already high, i.e., where pH is lowest (Fig 3.3a,d). The former can be largely understood from the fact that the highest rates with which $[CO_3^{2-}]$ is titrated away from the invasion of C_{ant} through the short-circuit reaction $CO_2 + CO_3^{2-} + H_2O = 2HCO_3^-$ (Sarmiento & Gruber, 2006) occurs in the regions where $[CO_3^{2-}]$ is most abundant, i.e. where Ω_{ar} is highest. The latter is directly the inverse, i.e., the regions where most of the invading C_{ant} is not titrated away but rather stay in its acid form through reaction with water to form H_2CO_3 is where $[CO_3^{2-}]$ (and hence also Ω_{ar}) is the lowest, and where $[H^+]$ is highest (or pH lowest).

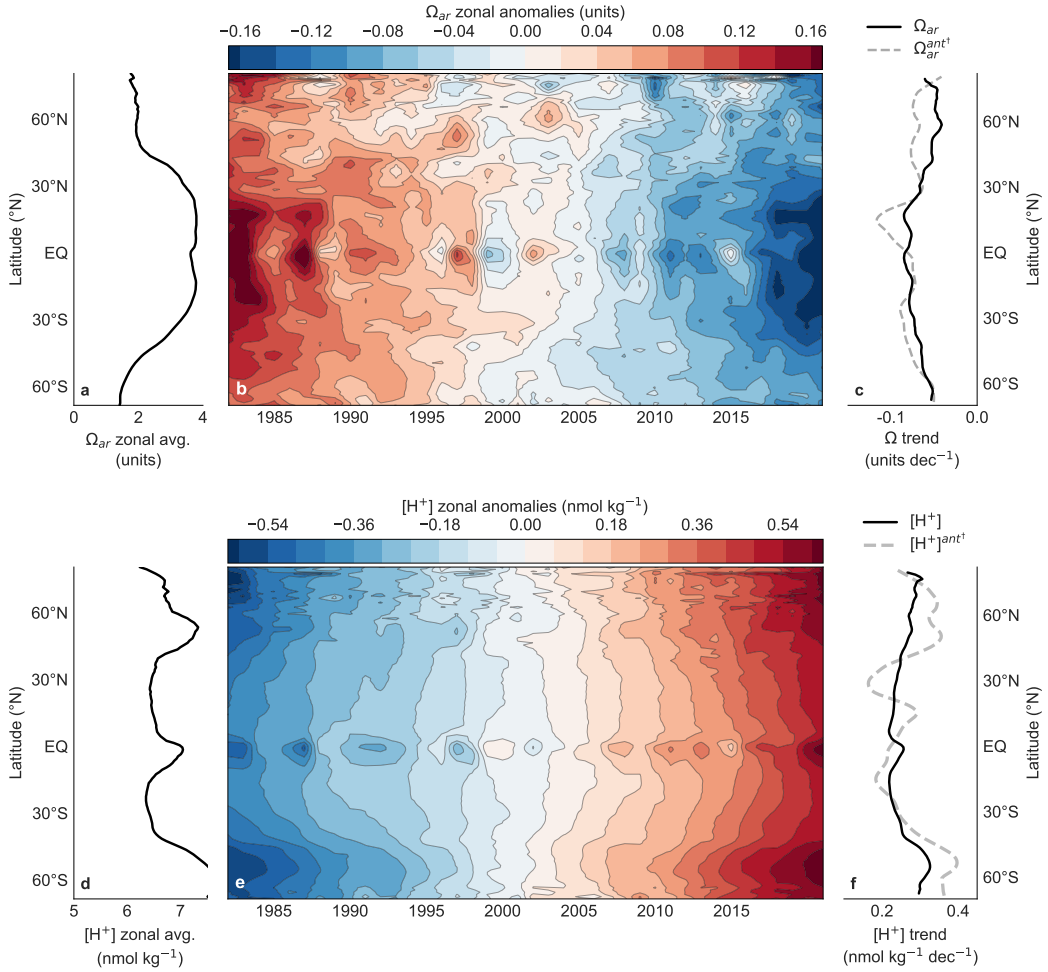

Figure 3. Hovmoeller (latitude-time) diagrams of the zonally averaged anomalies from 1982 to 2021 together with their long-term averages and zonal mean trends. (a) Zonal average of the long-term mean Ω_{ar}. (b) Hovmoeller diagram of the zonally averaged anomalies of Ω_{ar}. The anomalies have been computed relative to the long-term mean shown in (a). (c) Zonal average of the long-term linear trend in Ω_{ar} (solid line) together with the trend estimated solely on the basis of the estimated increase in anthropogenic CO2 (dashed line). (d) As (a), but for $[H^+]$. (e), as (b) but for $[H^+]$. (f), as (c) but for $[H^+]$.

3.4 Interannual Variability

In addition to the long-term trends, both Ω_{ar} and $[H^+]$ are subject to a substantial amount of interannual variability Fig. 3.3, with Ω_{ar} revealing a much more variable pattern than $[H^+]$. The interannual variability for $[H^+]$ is primarily confined to the equator, with distinct negative $[H^+]$ anomalies found around 1983, 1987, 1992, 1998, 2002, etc., i.e., years characterized by El Niño events in the tropical eastern Pacific. These negative $[H^+]$ anomalies are likely caused by the near cessation of upwelling during these events, thus bringing much less high DIC/low Alk (low $[H^+]$) waters to the surface, keeping surface $[H^+]$ low (and pH high). Even though these events are also characterized by higher than normal sea-surface temperatures, this effect appears to be overwhelmed by the low DIC concentrations that characterize El Niño events (McKinley et al., 2004; R. Feely et al., 2006). Positive anomalies in $[H^+]$ occur during La Niña events, when upwelling

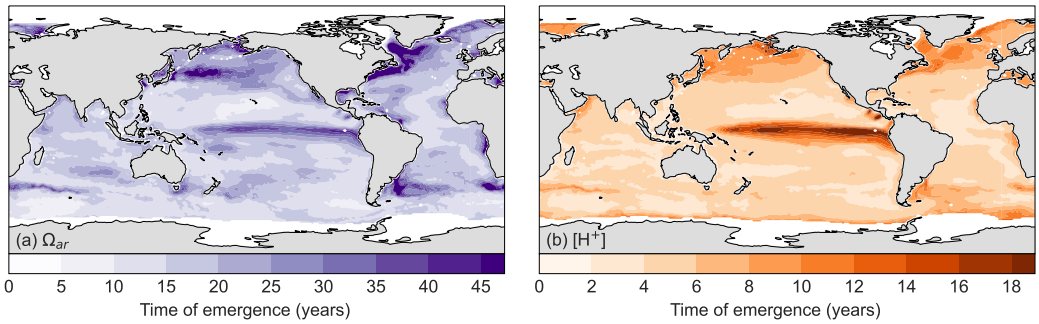

Figure 4. Maps depicting the time of emergence (ToE) for (a) Ω_{ar} and (b) pH. The ToE was estimated from the rates of change in Ω_{ar} and pH and variations in their respective deseasonalized monthly data, see eq(4) in the main text.

is strong, bringing large amounts of high DIC/low Alk waters to the surface(Sutton et al., 2014).

The Ω_{ar} anomalies at equatorial latitudes are the opposite of those of $[H^+]$, i.e., Ω_{ar} tends to be anomalously high during El Niño events and anomalously low during La Niña events. The drivers are the same as those for $[H^+]$, i.e., variations in the strength of upwelling that tends to bring high DIC/low Alk (low Ω_{ar}) waters to the surface.

The Hovmoeller plot for Ω_{ar} reveals also a substantial amount of interannual variability in the extratropics, especially when compared to $[H^+]$ (contrast Fig. 3.3b with panel f). The variability in the zonal mean comes from all ocean basins. It is most likely related to the interaction of transport/mixing and biological production that tend to change Ω_{ar} in opposite direction. Their effect is not dampened by co-variations with temperature, since temperature plays a relatively marginal role in controlling Ω_{ar}. This situation tends to differ for $[H^+]$, where surface warming/cooling often dampens the effects of transport/mixing and biological production, leading to a lower level of variability (see also Jiang et al. (2019)).

3.5 Time of Emergence

Across the global ocean, the times of emergence (ToE) for both Ω_{ar} and pH estimated from OceanSODA-ETHZ are on the scale of years to decades (Fig. 4), but with large regional differences between the two parameters. The ToE of Ω_{ar} ranges from a value of near 1 year up to nearly 50 years while that of pH ranges from near 1 year to around 20 years only. However, for the majority of the open oceans, ToE of both Ω_{ar} and pH is on the time scales of a few years to a decade. Ω_{ar} exhibits generally longer ToE than pH in most locations, especially in the Northern Hemisphere, largely caused by the higher level of variability in Ω_{ar} shown in Fig. 3.3. For both Ω_{ar} and pH, the eastern equatorial Pacific is estimated to have one of the longest ToE (decade to several decades), since this is the region where both parameters vary interannually the most. For Ω_{ar}, ToE is also long in the mid to high-latitude oceans, including the high-latitude north Pacific, north Atlantic, and south Atlantic.

These findings imply that at most within half a century, the underlying trends in Ω_{ar} and $[H^+]$ will become strong enough to exceed their interannual variability for most of the open oceans. Correlation between the ToE distributions of these two OA parameters also indicates that the development of acidification can be easily detected amidst interannual variations in a time frame of a few decades for vast regions of the global oceans.

Our estimate of the ToE compares well with those that have been estimated from models so far (Schlunegger et al., 2019; Rodgers et al., 2015; Keller et al., 2014; Friedrich et al., 2012), although differences in the definition make direct quantifications difficult. For example, Friedrich et al. (2012) used the amplitude of the seasonal cycle as the metric of variance, whereas we use here the standard deviation of the deseasonalized data, i.e., we consider primarily the level of interannual variability as the "noise" against which we aim to detect the signal. Schlunegger et al. (2019) and Rodgers et al. (2015) used the "noise" from an ensemble of models and compared that to the trend emerging from the ensemble mean, which is closer to our definition, but still different. Despite these important differences, our work here confirms prior assessments that the signals from ocean acidification emerge relatively fast, i.e., on the order of years to decades, from the background noise. Our results also confirm prior findings that the equatorial Pacific has one of the longest ToEs(Rodgers et al., 2015). Previously not discussed was the difference between pH and Ω_{ar}, which we are now able to show.

3.6 Caveats and limitations

We note that the interannual variability of pH, $[H^+]$, and Ω_{ar} in the OceanSODA-ETHZ product may be underestimated. We base this potential caveat on the observation that the variability of the pCO_2 data in OceanSODA-ETHZ is on the low end compared to that exhibited in six other surface ocean pCO_2 products (Table S5 in supplementary). Comparison of zonally averaged interannual variability of pCO_2 between the OceanSODA-ETHZ data set (lowest interannual variability of the seven products) and six other pCO_2-products suggests that the largest discrepancy in their respective interannual variability estimates exists in the high latitudes (Fig. S6 in supplementary). A systematically low interannual variability in the OceanSODA-ETHZ product would directly lead to a systematic underestimation of the ToE. Thus, we conclude that our ToE results may be biased low, although we suspect that this systematic underestimation of the variability would not alter the regional differences.

In addition, we also note that our driver decomposition could be biased since we use the same variables as predictors for generating the fields in the first place and for diagnosing the decomposition in the second place. This is potentially problematic since the predictors are interdependent, especially SST and SSS. While this may not cause problems when predicting the distribution of the variables, it may be problematic when diagnosing the role of freshwater forcing and heating/cooling of the sea surface. We currently do not know how to address this, but we also do not have any evidence that this is an issue. Still, one needs to be aware of this potential caveat when analyzing the driver decomposition.

4 Summary and Conclusions

Our analyses of the OceanSODA-ETHZ product suggest that global surface ocean Ω_{ar} and pH have declined over the past 4 decades at rates of -0.071 $\pm$ 0.001 and -0.0170 $\pm$ 0.0001 units per decade, respectively. Both trends are predominantly caused by the increase in atmospheric CO_2 driving a trend in the surface ocean concentration of anthropogenic CO_2. But we also showed that a decrease in the surface ocean concentration of natural CO_2 and ocean warming modulate the trends measurably. Especially noteworthy is the $\sim$15% enhancement of the pH trend by ocean warming. ENSO dominates the interannual variability in both Ω_{ar} and pH, although Ω_{ar} has greater interannual variability. This leads to a substantially longer time of emergence for Ω_{ar} (several decades) compared to pH (around a decade).

Our global trend analyses represent a major step forward relative to prior data-based assessments of the global trends in OA, which were either based on a limited number of time series stations (Canadell et al., 2021) or based on spatial aggregation of data

over large-scale biomes (Lauvset et al., 2015). Not only were we able to substantially reduce the uncertainties of the trends, but we also pointed out the substantial regional differences in the trends of the most important OA parameters with pH experiencing, on average, the highest rates of changes in the higher latitudes, while the largest changes in Ω_{ar} are found in the tropics. These regional differences need to be taken into account when assessing the impact of OA across the global surface ocean. For example, the especially high rates of change in Ω_{ar} in the eastern Pacific can bring warm-water corals in toward critical saturation thresholds (Hoegh-Guldberg et al., 2007) much faster than inferred from the globally averaged rate of change of Ω_{ar}. Our observation-based analyses can provide also important evaluation constraints for model studies used to project OA into the future (Kwiatkowski et al., 2020). Of particular concern is again the spatial structure of the simulated changes, an aspect that has not been given a lot of attention so far.

Understanding the long-term trends and variability of global acidification enables us to put local changes into the larger context of global trends and variability. Even though we emphasized here the role of other drivers, the main driver of OA is the increase in atmospheric CO_2. Thus, unless the anthropogenic emissions of CO_2 are massively curtailed, OA is bound to continue, increasing its threats on marine life (Kroeker et al., 2013; Bindoff et al., 2019).

Acknowledgments

This research has been supported by the European Space Agency (OceanSODA project, grant no. 4000112091/14/I-LG), and by the European Commission through its Horizon 2020 research and innovation programme under grant agreements no. 821003 (project 4C) and no. 820989 (COMFORT).

References

Bates, N. R. (2007). Interannual variability of the oceanic CO_2 sink in the subtropical gyre of the North Atlantic Ocean over the last 2 decades. *Journal of Geophysical Research: Oceans*, *112*(C9).

Bates, N. R., Astor, Y. M., Church, M. J., Currie, K., Dore, J. E., González-Dávila, M., ... Santana-Casiano, J. M. (2014). A time-series view of changing surface ocean chemistry due to ocean uptake of anthropogenic CO_2 and ocean acidification. *Oceanography*, *27*(1), 126–141.

Bates, N. R., & Johnson, R. J. (2020). Acceleration of ocean warming, salinification, deoxygenation and acidification in the surface subtropical north atlantic ocean. *Communications Earth & Environment*, *1*(1), 33.

Bindoff, N. L., Cheung, W. W., Kairo, J. G., Arístegui, J., Guinder, V. A., Hallberg, R., ... others (2019). Changing ocean, marine ecosystems, and dependent communities. *IPCC special report on the ocean and cryosphere in a changing climate*, 477–587.

Bopp, L., Resplandy, L., Orr, J. C., Doney, S. C., Dunne, J. P., Gehlen, M., ... others (2013). Multiple stressors of ocean ecosystems in the 21st century: projections with CMIP5 models. *Biogeosciences*, *10*(10), 6225–6245.

Boutin, J., Vergely, J.-L., Marchand, S., d'Amico, F., Hasson, A., Kolodziejczyk, N., ... Vialard, J. (2018). New smos sea surface salinity with reduced systematic errors and improved variability. *Remote Sensing of Environment*, *214*, 115–134.

Boyer, T. P., Garcia, H. E., Locarnini, R. A., Zweng, M. M., Mishonov, A. V., Reagan, J. R., ... Smolyar, I. V. (2018). World Ocean Atlas 2018. *NOAA National Centers for Environmental Information*.

Brewer, P. G. (2013). A short history of ocean acidification science in the 20th cen-

tury: a chemist's view. *Biogeosciences*, *10*(11), 7411–7422.

Byrne, R. H., & Breland, J. A. (1989). High precision multiwavelength pH determinations in seawater using cresol red. *Deep Sea Research Part A. Oceanographic Research Papers*, *36*(5), 803–810.

Caldeira, K., & Wickett, M. E. (2003). Anthropogenic carbon and ocean ph. *Nature*, *425*(6956), 365–365. Retrieved from `https://doi.org/10.1038/425365a` doi: 10.1038/425365a

Canadell, J. G., Monteiro, P. M., Costa, M. H., Da Cunha, L. C., Cox, P. M., Alexey, V., ... others (2021). *Global carbon and other biogeochemical cycles and feedbacks.*

Carton, J. A., Chepurin, G. A., & Chen, L. (2018). SODA3: A new ocean climate reanalysis. *Journal of Climate*, *31*(17), 6967–6983.

Chau, T. T. T., Gehlen, M., & Chevallier, F. (2022). A seamless ensemble-based reconstruction of surface ocean pCO_2 and air–sea CO_2 fluxes over the global coastal and open oceans. *Biogeosciences*, *19*(4), 1087–1109.

Claustre, H., Johnson, K. S., & Takeshita, Y. (2020). Observing the global ocean with biogeochemical-argo. *Annual review of Marine science*, *12*, 23–48.

Clayton, T. D., & Byrne, R. H. (1993). Spectrophotometric seawater pH measurements: total hydrogen ion concentration scale calibration of m-cresol purple and at-sea results. *Deep Sea Research Part I: Oceanographic Research Papers*, *40*(10), 2115–2129.

Clement, D., & Gruber, N. (2018). The eMLR(C*) method to determine decadal changes in the global ocean storage of anthropogenic CO_2. *Global Biogeochemical Cycles*, *32*(4), 654–679. Retrieved from `http://doi.wiley.com/10.1002/2017GB005819https://onlinelibrary.wiley.com/doi/10.1002/2017GB005819` doi: 10.1002/2017GB005819

Cornwall, C. E., Comeau, S., Kornder, N. A., Perry, C. T., van Hooidonk, R., DeCarlo, T. M., ... others (2021). Global declines in coral reef calcium carbonate production under ocean acidification and warming. *Proceedings of the National Academy of Sciences*, *118*(21).

Cornwall, C. E., Harvey, B. P., Comeau, S., Cornwall, D. L., Hall-Spencer, J. M., Peña, V., ... Porzio, L. (2022). Understanding coralline algal responses to ocean acidification: Meta-analysis and synthesis. *Global Change Biology*, *28*(2), 362–374.

DeVries, T. (2014). The oceanic anthropogenic CO_2 sink: Storage, air-sea fluxes, and transports over the industrial era. *Global Biogeochemical Cycles*, *28*(7), 631–647.

Dickson, A., & Millero, F. J. (1987). A comparison of the equilibrium constants for the dissociation of carbonic acid in seawater media. *Deep Sea Research Part A. Oceanographic Research Papers*, *34*(10), 1733–1743.

Dickson, A. G. (1993). The measurement of seawater pH. *Marine Chemistry*, *44*(2-4), 131–142.

Dlugokencky, E., Thoning, K., Lan, X., & Tans, P. (2021). *NOAA greenhouse gas reference from atmospheric carbon dioxide dry air mole fractions from the NOAA GML carbon cycle cooperative global air sampling network.*

Doney, S. C., Busch, D. S., Cooley, S. R., & Kroeker, K. J. (2020). The impacts of ocean acidification on marine ecosystems and reliant human communities. *Annual Review of Environment and Resources*, *45*, 83–112.

Doney, S. C., Fabry, V. J., Feely, R. A., & Kleypas, J. A. (2009). Ocean acidification: the other CO_2 problem. *Annual review of marine science*, *1*, 169–192.

Dore, J. E., Lukas, R., Sadler, D. W., Church, M. J., & Karl, D. M. (2009). Physical and biogeochemical modulation of ocean acidification in the central North Pacific. *Proceedings of the National Academy of Sciences*, *106*(30), 12235–12240.

Egleston, E. S., Sabine, C. L., & Morel, F. M. (2010). Revelle revisited: Buffer factors that quantify the response of ocean chemistry to changes in DIC and

alkalinity. *Global Biogeochemical Cycles*, *24*(1).

Fay, A., & McKinley, G. (2013). Global trends in surface ocean pCO_2 from in situ data. *Global Biogeochemical Cycles*, *27*(2), 541–557.

Fay, A. R., Gregor, L., Landschützer, P., McKinley, G. A., Gruber, N., Gehlen, M., ... others (2021). SeaFlux: harmonization of air–sea CO_2 fluxes from surface pCO_2 data products using a standardized approach. *Earth System Science Data*, *13*(10), 4693–4710.

Feely, R., Takahashi, T., Wanninkhof, R., McPhaden, M., Cosca, C., Sutherland, S., & Carr, M.-E. (2006). Decadal variability of the air-sea CO_2 fluxes in the equatorial Pacific Ocean. *Journal of Geophysical Research: Oceans*, *111*(C8).

Feely, R. A., Doney, S. C., & Cooley, S. R. (2009). Ocean acidification: Present conditions and future changes in a high-CO_2 world. *Oceanography*, *22*(4), 36–47.

Feely, R. A., Sabine, C. L., Lee, K., Berelson, W., Kleypas, J., Fabry, V. J., & Millero, F. J. (2004). Impact of anthropogenic CO_2 on the $CaCO_3$ system in the oceans. *Science*, *305*(5682), 362–366.

Figuerola, B., Hancock, A. M., Bax, N., Cummings, V. J., Downey, R., Griffiths, H. J., ... Stark, J. S. (2021). A review and meta-analysis of potential impacts of ocean acidification on marine calcifiers from the Southern Ocean. *Frontiers in Marine Science*, *8*, 24.

Friedlingstein, P., Jones, M. W., O'Sullivan, M., Andrew, R. M., Bakker, D. C., Hauck, J., ... others (2022). Global carbon budget 2021. *Earth System Science Data*, *14*(4), 1917–2005.

Friedrich, T., Timmermann, A., Abe-Ouchi, A., Bates, N., Chikamoto, M., Church, M., ... others (2012). Detecting regional anthropogenic trends in ocean acidification against natural variability. *Nature Climate Change*, *2*(3), 167–171.

Gloege, L., Yan, M., Zheng, T., & McKinley, G. A. (2022). Improved quantification of ocean carbon uptake by using machine learning to merge global models and pCO_2 data. *Journal of Advances in Modeling Earth Systems*, *14*(2), e2021MS002620.

Gregor, L., & Gruber, N. (2021). OceanSODA-ETHZ: a global gridded data set of the surface ocean carbonate system for seasonal to decadal studies of ocean acidification. *Earth System Science Data*, *13*(2), 777–808.

Gruber, N., Bakker, D. C., DeVries, T., Gregor, L., Hauck, J., Landschützer, P., ... Müller, J. D. (2023). Trends and variability in the ocean carbon sink. *Nature Reviews Earth & Environment*, 1–16.

Gruber, N., Bates, N. R., & Keeling, C. D. (2002, dec). Interannual variability in the North Atlantic carbon sink. *Science*, *298*(5602), 2374–2378. Retrieved from `http://www.ncbi.nlm.nih.gov/pubmed/12493911` doi: 10.1126/science.1077077

Gruber, N., Clement, D., Carter, B. R., Feely, R. A., Van Heuven, S., Hoppema, M., ... others (2019). The oceanic sink for anthropogenic CO_2 from 1994 to 2007. *Science*, *363*(6432), 1193–1199.

Gruber, N., Hauri, C., Lachkar, Z., Loher, D., Frölicher, T. L., & Plattner, G.-K. (2012). Rapid progression of ocean acidification in the California Current System. *Science*, *337*(6091), 220–223.

Hall-Spencer, J. M., & Harvey, B. P. (2019). Ocean acidification impacts on coastal ecosystem services due to habitat degradation. *Emerging Topics in Life Sciences*, *3*(2), 197–206.

Harvey, B. P., Kon, K., Agostini, S., Wada, S., & Hall-Spencer, J. M. (2021). Ocean acidification locks algal communities in a species-poor early successional stage. *Global Change Biology*, *27*(10), 2174–2187.

Hauck, J., Zeising, M., Le Quéré, C., Gruber, N., Bakker, D. C. E., Bopp, L., ... Séférian, R. (2020, oct). Consistency and Challenges in the Ocean Carbon Sink Estimate for the Global Carbon Budget. *Frontiers in Marine Science*, *7*(October), 1–33. Retrieved from `https://www.frontiersin.org/articles/`

10.3389/fmars.2020.571720/full doi: 10.3389/fmars.2020.571720

Hoegh-Guldberg, O., Mumby, P. J., Hooten, A. J., Steneck, R. S., Greenfield, P., Gomez, E., ... Hatziolos, M. E. (2007, 12). Coral reefs under rapid climate change and ocean acidification. *Science*, *318*, 1737-1742. Retrieved from https://www.science.org/doi/10.1126/science.1152509 doi: 10.1126/science.1152509

Humphreys, M. P., Gregor, L., Pierrot, D., van Heuven, S., Lewis, E. R., & Wallace, D. W. (2020). *PyCO2SYS: marine carbonate system calculations in Python.* Retrieved from https://doi.org/10.5281/zenodo.3967359{\#}.XzJOEdRZo2g.mendeley doi: 10.5281/ZENODO.3967359

Ishii, M., Rodgers, K. B., Inoue, H. Y., Toyama, K., Sasano, D., Kosugi, N., ... others (2020). Ocean acidification from below in the tropical pacific. *Global Biogeochemical Cycles*, *34*(8), e2019GB006368.

Jiang, L.-Q., Carter, B. R., Feely, R. A., Lauvset, S. K., & Olsen, A. (2019). Surface ocean pH and buffer capacity: past, present and future. *Scientific reports*, *9*(1), 1–11.

Johnson, G. C., & Lyman, J. M. (2020). Warming trends increasingly dominate global ocean. *Nature Climate Change*, *10*(8), 757–761. Retrieved from https://doi.org/10.1038/s41558-020-0822-0 doi: 10.1038/s41558-020-0822-0

Keller, K. M., Joos, F., & Raible, C. C. (2014). Time of emergence of trends in ocean biogeochemistry. *Biogeosciences*, *11*(13), 3647–3659.

Khatiwala, S., Tanhua, T., Mikaloff Fletcher, S., Gerber, M., Doney, S. C., Graven, H. D., ... others (2013). Global ocean storage of anthropogenic carbon. *Biogeosciences*, *10*(4), 2169–2191.

Kim, J.-Y., Kang, D.-J., Lee, T., & Kim, K.-R. (2014). Long-term trend of CO_2 and ocean acidification in the surface water of the Ulleung Basin, the East Japan Sea inferred from the underway observational data. *Biogeosciences*, *11*(9), 2443–2454.

Kroeker, K. J., Kordas, R. L., Crim, R., Hendriks, I. E., Ramajo, L., Singh, G. S., ... Gattuso, J.-P. (2013). Impacts of ocean acidification on marine organisms: quantifying sensitivities and interaction with warming. *Global change biology*, *19*(6), 1884–1896.

Kwiatkowski, L., Torres, O., Bopp, L., Aumont, O., Chamberlain, M., Christian, J. R., ... others (2020). Twenty-first century ocean warming, acidification, deoxygenation, and upper-ocean nutrient and primary production decline from CMIP6 model projections. *Biogeosciences*, *17*(13), 3439–3470.

Landschützer, P., Gruber, N., & Bakker, D. C. (2016). Decadal variations and trends of the global ocean carbon sink. *Global Biogeochemical Cycles*, *30*(10), 1396–1417.

Landschützer, P., Gruber, N., Bakker, D. C., & Schuster, U. (2014). Recent variability of the global ocean carbon sink. *Global Biogeochemical Cycles*, *28*(9), 927–949.

Landschützer, P., Gruber, N., Bakker, D. C., Stemmler, I., & Six, K. D. (2018). Strengthening seasonal marine CO_2 variations due to increasing atmospheric CO_2. *Nature Climate Change*, *8*(2), 146–150.

Lauvset, S. K., & Gruber, N. (2014). Long-term trends in surface ocean ph in the north atlantic. *Marine Chemistry*, *162*, 71–76.

Lauvset, S. K., Gruber, N., Landschützer, P., Olsen, A., & Tjiputra, J. (2015). Trends and drivers in global surface ocean pH over the past 3 decades. *Biogeosciences*, *12*(5), 1285–1298.

Leseurre, C., Monaco, C. L., Reverdin, G., Metzl, N., Fin, J., Mignon, C., & Benito, L. (2022). Trends and drivers of sea surface fCO_2 and pH changes observed in the Southern Indian Ocean over the last two decades (1998–2019). *Biogeosciences*, *19*, 2599–2625.

Lewis, E., Wallace, D., & Allison, L. J. (1998). *Program developed for CO_2 system calculations* (Tech. Rep.). Brookhaven National Laboratory, Department of Applied Science, Upton, NY, United States.

Lovenduski, N. S., Gruber, N., Doney, S. C., & Lima, I. D. (2007). Enhanced CO_2 outgassing in the Southern Ocean from a positive phase of the Southern Annular Mode. *Global Biogeochemical Cycles*, *21*(2).

Matsumoto, K., & Gruber, N. (2005). How accurate is the estimation of anthropogenic carbon in the ocean? an evaluation of the ΔC^* method. *Global Biogeochemical Cycles*, *19*(3).

McKinley, G. A., Follows, M. J., & Marshall, J. (2004). Mechanisms of air-sea CO_2 flux variability in the equatorial Pacific and the North Atlantic. *Global Biogeochemical Cycles*, *18*(2).

McNeil, B., & Matear, R. (2013). The non-steady state oceanic CO_2 signal: its importance, magnitude and a novel way to detect it. *Biogeosciences*, *10*(4), 2219–2228.

Mehrbach, C., Culberson, C., Hawley, J., & Pytkowicx, R. (1973). Measurement of the apparent dissociation constants of carbonic acid in seawater at atmospheric pressure 1. *Limnology and oceanography*, *18*(6), 897–907.

Mikaloff Fletcher, S. E., Gruber, N., Jacobson, A. R., Doney, S. C., Dutkiewicz, S., Gerber, M., ... others (2006). Inverse estimates of anthropogenic CO_2 uptake, transport, and storage by the ocean. *Global biogeochemical cycles*, *20*(2).

Mucci, A., et al. (1983). The solubility of calcite and aragonite in seawater at various salinities, temperatures, and one atmosphere total pressure. *American Journal of Science*, *283*(7), 780–799.

Olafsson, J., Olafsdottir, S., Benoit-Cattin, A., & Takahashi, T. (2010). The Irminger Sea and the Iceland Sea time series measurements of sea water carbon and nutrient chemistry 1983–2008. *Earth System Science Data*, *2*(1), 99–104.

Orr, J. C. (2011). Recent and future changes in ocean carbonate chemistry. *Ocean acidification*, *1*, 41–66.

Orr, J. C., Fabry, V. J., Aumont, O., Bopp, L., Doney, S. C., Feely, R. A., ... others (2005). Anthropogenic ocean acidification over the twenty-first century and its impact on calcifying organisms. *Nature*, *437*(7059), 681–686.

Radford, C., Collins, S., Munday, P., & Parsons, D. (2021). Ocean acidification effects on fish hearing. *Proceedings of the Royal Society B*, *288*(1946), 20202754.

Raimondi, L., Matthews, J. B. R., Atamanchuk, D., Azetsu-Scott, K., & Wallace, D. W. (2019). The internal consistency of the marine carbon dioxide system for high latitude shipboard and in situ monitoring. *Marine Chemistry*, *213*, 49–70.

Reynolds, R. W., Smith, T. M., Liu, C., Chelton, D. B., Casey, K. S., & Schlax, M. G. (2007). Daily high-resolution-blended analyses for sea surface temperature. *Journal of climate*, *20*(22), 5473–5496.

Rödenbeck, C., Bakker, D. C., Gruber, N., Iida, Y., Jacobson, A. R., Jones, S., ... others (2015). Data-based estimates of the ocean carbon sink variability–first results of the Surface Ocean pCO_2 Mapping intercomparison (SOCOM). *Biogeosciences*, *12*, 7251–7278.

Rodgers, K. B., Lin, J., & Frölicher, T. L. (2015). Emergence of multiple ocean ecosystem drivers in a large ensemble suite with an Earth system model. *Biogeosciences*, *12*(11), 3301–3320.

Sabine, C. L., Feely, R. A., Gruber, N., Key, R. M., Lee, K., Bullister, J. L., ... others (2004). The oceanic sink for anthropogenic CO_2. *Science*, *305*(5682), 367–371.

Sallée, J.-B., Pellichero, V., Akhoudas, C., Pauthenet, E., Vignes, L., Schmidtko, S., ... Kuusela, M. (2021). Summertime increases in upper-ocean stratification

and mixed-layer depth. *Nature*, *591*(7851), 592–598.

Sarmiento, J., & Gruber, N. (2006). *Ocean biogeochemical dynamics*. Princeton University Press.

Schlunegger, S., Rodgers, K. B., Sarmiento, J. L., Frölicher, T. L., Dunne, J. P., Ishii, M., & Slater, R. (2019). Emergence of anthropogenic signals in the ocean carbon cycle. *Nature climate change*, *9*(9), 719–725.

Sutton, A. J., Feely, R. A., Sabine, C. L., McPhaden, M. J., Takahashi, T., Chavez, F. P., ... Mathis, J. T. (2014). Natural variability and anthropogenic change in equatorial Pacific surface ocean pCO_2 and pH. *Global Biogeochemical Cycles*, *28*(2), 131–145.

Takahashi, T., Sutherland, S. C., Chipman, D. W., Goddard, J. G., Ho, C., Newberger, T., ... Munro, D. (2014). Climatological distributions of pH, pCO_2, total CO_2, alkalinity, and $CaCO_3$ saturation in the global surface ocean, and temporal changes at selected locations. *Marine Chemistry*, *164*, 95–125.

Terhaar, J., Frölicher, T. L., & Joos, F. (2023). Ocean acidification in emission-driven temperature stabilization scenarios: the role of TCRE and non-CO_2 greenhouse gases. *Environmental Research Letters*.

Tilbrook, B., Jewett, E. B., DeGrandpre, M. D., Hernandez-Ayon, J. M., Feely, R. A., Gledhill, D. K., ... others (2019). An enhanced ocean acidification observing network: from people to technology to data synthesis and information exchange. *Frontiers in Marine Science*, 337.

Tjiputra, J. F., Olsen, A., Bopp, L., Lenton, A., Pfeil, B., Roy, T., ... Heinze, C. (2014). Long-term surface pCO_2 trends from observations and models. *Tellus B: Chemical and Physical Meteorology*, *66*(1), 23083.

Weiss, R. (1974). Carbon dioxide in water and seawater: The solubility of non-ideal gas. *Marine Chemistry*, *2*, 203–215.

Observation-based trends and drivers of global surface ocean acidification over the past four decades

Danling Ma[1], Luke Gregor[1], and Nicolas Gruber[1]

[1]Environmental Physics, Institute of Biogeochemistry and Pollutant Dynamics, ETH Zurich, Zürich, Switzerland.

Key Points:

- From 1982 through 2021, surface ocean Ω_{ar} and pH declined at -0.071 ± 0.001 and -0.0170 ± 0.0001 per decade, respectively.
- These trends are predominantly caused by rising atmospheric CO2, with ocean warming enhancing the pH trend.
- ENSO dominates the interannual variability in Ω_{ar} and pH, although Ω_{ar} exhibits greater interannual variability.

Corresponding author: Nicolas Gruber, nicolas.gruber@env.ethz.ch

Abstract

The oceans are acidifying in response to the oceanic uptake of anthropogenic CO_2 from the atmosphere, yet the global-scale progression of this acidification has been poorly documented so far by observations. Here, we fill this gap and use an observation-based product, OceanSODA-ETHZ, to determine the trends and drivers of the surface ocean aragonite saturation state (Ω_{ar}) and pH over the last four decades (1982-2021). In the global mean, Ω_{ar} and pH declined at rates of -0.071 $\pm$ 0.001 decade^{-1} and -0.0170 $\pm$ 0.0001 decade^{-1}, respectively. These trends are driven primarily by the increase in the surface ocean concentration of dissolved inorganic carbon (DIC) in response to the uptake of anthropogenic CO_2, but moderated by changes in natural DIC. Surface warming enhances the decrease in pH, accounting for $\sim$ 15% of the global trend. Substantial ENSO-driven interannual variability is superimposed on these trends, with Ω_{ar} showing greater variability than pH.

Plain Language Summary

As the ocean takes up human-made CO_2 from the atmosphere, it becomes more acidic, i.e., its pH is dropping and so is its saturation state (Ω_{ar}) with respect to aragonite, a type of carbonate mineral. These chemical changes, generally referred to as "Ocean Acidification", are harming marine organisms. Here, we use an observation-based data set to investigate the trends and drivers of these two important metrics of acidification in global surface ocean over the last four decades (1982-2021). Our results confirm that pH and Ω_{ar} have been declining across the global ocean during the study period and that these trends are predominantly driven by the increase in the surface ocean concentration of dissolved inorganic carbon resulting from the accumulation of human-made CO_2. We also show that the observed ocean warming enhances the decline in pH. Both metrics, and especially Ω_{ar} vary substantially around these long-term trends, largely in response to El Niño events in the tropics. Our study provides, for the first time, a global observation-based quantification of the progression and driving factors of ocean acidification, which will help to better understand the impact of ocean acidification on marine life.

1 Introduction

The oceans provide a large ecosystem service by taking up roughly a third of the CO_2 emitted by anthropogenic activities (Friedlingstein et al., 2022; Sabine et al., 2004; Khatiwala et al., 2013; Gruber et al., 2023), but this comes at a substantial cost, i.e., ocean acidification (OA) (Caldeira & Wickett, 2003; Orr et al., 2005; Doney et al., 2009). While the term acidification stems from the fact that CO_2 taken up from the atmosphere and added to seawater liberates protons, i.e., increases the concentration of H^+ and thus lowers seawater pH (pH = -log [H^+]), OA refers to a larger set of chemical changes in seawater. Some of the CO_2 that is taken up is titrated away by carbonate ions dissolved in seawater (Sarmiento & Gruber, 2006), reducing the concentration of these ions. This causes the saturation state of calcium carbonate $CaCO_3$ minerals (Ω), such as that of aragonite (Ω_{ar}), to decline.

Ocean acidification has been the subject of much research in the past two decades since it can severely impact marine life (R. A. Feely et al., 2004; Orr et al., 2005; Doney et al., 2009; Gruber et al., 2012; Jiang et al., 2019; Kroeker et al., 2013). This impact can occur at the level of an individual organism by affecting, e.g., its physiology or behavioral patterns (Doney et al., 2020; Figuerola et al., 2021; Radford et al., 2021; Cornwall et al., 2022). It can also occur all the way up at the scales of communities and ecosystems, e.g., by altering population dynamics or by knocking out keystone species and thereby altering community structure (Hall-Spencer & Harvey, 2019; Doney et al., 2020; Corn-

wall et al., 2021; Harvey et al., 2021). Thus, it is critical that we understand the historical progression and contemporary state of OA across the global ocean. This would permit us also to make better predictions of what the future may hold. However, the ability of the oceanographic community to quantitatively describe the past progression of OA across the global ocean with observations has been remarkably limited. This contrasts with model-based studies which clearly established past and future trends of OA (Orr et al., 2005; R. A. Feely et al., 2009; Friedrich et al., 2012; Bopp et al., 2013; Kwiatkowski et al., 2020; Terhaar et al., 2023).

This lack of observation-based studies of OA trends is in part due to the limited number of historical observations available for the key parameters of OA, i.e., $[H^+]$, pH, and Ω_{ar}. For example, seawater pH measurements before 1989 relied primarily on glass electrodes, which involve uncertainties of the order of 0.1 pH units. This is too uncertain to capture the pH alterations induced by OA, rendering these observations unusable. A further complication arises because the pH scale of many earlier records is ambiguous (Jiang et al., 2019). The availability and quality of seawater pH data has improved gradually in the subsequent decades, following the refinement of spectrophotometric pH measurement methods (Byrne & Breland, 1989; Clayton & Byrne, 1993; A. G. Dickson, 1993; Jiang et al., 2019). These developments have been greatly aided by efforts such as the Global Ocean Acidification Observing Network (GOA-ON) (Brewer, 2013; Tilbrook et al., 2019), which supported communities around the world to make high quality measurements, especially in coastal regions. Also, the recent advent of the biogeochemical Argo program with pH sensors has dramatically increased the amount of available data in the last few years, especially in the open seas (Claustre et al., 2020). But the temporal coverage of these data is very limited, preventing an assessment of OA changes over multiple decades. For the saturation state Ω_{ar} or the concentration of the carbonate ion in seawater, the situation is even worse, as they are typically not measured directly. This leaves no record from which changes in time can be deduced directly.

For these reasons, observation-based OA trend studies have used pH, $[H^+]$, and Ω_{ar} computed from the more frequently measured variables of the ocean carbonate system, namely the partial pressure of CO_2 (pCO_2) and total alkalinity (Alk) (Bates, 2007; Bates et al., 2014; Lauvset & Gruber, 2014; Lauvset et al., 2015; Jiang et al., 2019). Most studies so far have applied this approach for local to regional studies, relying primarily on the data from the few existing long-term time series sites (Bates, 2007; Bates et al., 2014; Olafsson et al., 2010) or the few regions where sufficient observations exist to establish trends directly (Sutton et al., 2014; Kim et al., 2014; Leseurre et al., 2022). These studies unequivocally demonstrated that the ocean is acidifying, revealing highly significant long-term decreases in pH and Ω_{ar} at all sites and regions. But the community lacks an observation-based global-scale analysis that permits researchers to put these local and regional trends into context and also allows them to assess regional differences.

A first attempt to establish global trends in OA based solely on observations was made by Lauvset et al. (2015) who used measured pCO_2 and empirical estimates of Alk to estimate trends in surface ocean pH. They found significant pH decreases in ∼70% of all large-scale biomes and a mean rate of decrease of 0.018 ± 0.004 decade^{-1} for 1991–2011. But their study did not include Ω_{ar}, had insufficient data in several key regions such as the Southern Ocean, required a large amount of spatial aggregation leading to a very low resolution, and was limited in time to two decades. Building on this work and its own synthesis of the data from various time series sites across the world's oceans, the Intergovernmental Panel on Climate Change (IPCC) concluded in its special report on the Ocean and Cryosphere (Bindoff et al., 2019), that "pH in open ocean surface water has changed by a virtually certain range of –0.017 to –0.027 pH units per decade since the late 1980s." IPCC's Working Group 1 report in AR6 confirmed in essence this very large range for the global mean rate, and also discussed the spatial variability around this mean trend (Canadell et al., 2021). An alternative approach was taken more recently

by Jiang et al. (2019) who combined a climatological seawater CO_2 product with model results to obtain trends in the OA parameters. But by relying on a model for establishing the trends, this estimate cannot really be considered observation-based. Thus, while there is a pressing need for an observation-based assessment of the trends and drivers of OA on a global scale, the existing analyses are insufficient to fulfil this need. This gap is even more evident when compared to the huge volume of literature on long-term trends and variability in surface ocean pCO_2 (A. Fay & McKinley, 2013; Tjiputra et al., 2014; Landschützer et al., 2014; Rödenbeck et al., 2015; Landschützer et al., 2016; A. R. Fay et al., 2021; Gloege et al., 2022).

To close this gap, we present a global-scale analysis on the trends and drivers in both surface ocean pH and Ω_{ar} using an updated version of the OceanSODA-ETHZ observation-based product (Gregor & Gruber, 2021). This updated product covers the period from 1982 to 2021 at a spatial resolution of $1° \times 1°$, and at monthly resolution in time, and thus provides not only much higher resolution than the previous analysis by Lauvset et al. (2015), but also doubles the length of the analyzed time period. OceanSODA-ETHZ was derived by combining in-situ observations of pCO_2 and Alk with a range of satellite observations using a machine-learning approach. In this product, the surface ocean $[H^+]$, pH and Ω_{ar} are computed from the mapped pCO_2 and Alk data. Since this approach explicitly also involves the determination of the concentration of dissolved inorganic carbon (DIC), it permits us to analyze also the main drivers for the changes in $[H^+]$, pH and Ω_{ar}.

2 Materials and Methods

2.1 OceanSODA-ETHZ dataset and trend analyses

We use the global surface $[H^+]$, pH, and Ω_{ar} data from OceanSODA-ETHZ to analyze long-term trends in global OA from 1982 through 2021 (Gregor & Gruber, 2021). OceanSODA-ETHZ is an observation-based, global gridded data set with monthly data for ocean carbonate system parameters at a resolution of $1° \times 1°$. It was derived with a two-step machine learning approach (clustering and regression) that maps the observed distribution of pCO_2 and Alk to the global ocean using a range of independent variables as predictors. The version used here was updated from the published version by including data for the years 2020 and 2021. The OceanSODA-ETHZ product computed $[H^+]$, pH, Ω_{ar} and DIC from the mapped pCO_2 and Alk distribution by solving the marine carbonate system:

$$\Omega_{ar}, \mathrm{pH}, [H^+], DIC, \ldots = \mathrm{PyCO2SYS}(p\mathrm{CO}_2, Alk, T, S, Nutrients) \quad (1)$$

where PyCO2SYS is the software used to solve the marine carbonate system (Humphreys et al., 2020). For the dissociation constants of the marine carbonate system, we used the Mehrbach et al. (1973) constants refitted by A. Dickson and Millero (1987), as this gives the lowest uncertainty whenpCO_2 and Alk are used as input (Raimondi et al., 2019). Additional inputs consist of sea-surface temperature (T), sea-surface salinity (S), and the concentrations of the nutrients silicate and phosphate. Sea-surface temperature was taken from the NOAA OI SST V2 High-Resolution Dataset (OISSTv2; Reynolds et al., 2007), while sea-surface salinity is a combination of the ESA-CCI sea surface salinity product for 2010 to 2020 (Boutin et al., 2018) and Simple Ocean Data Assimilation (SODA v3.4.2; Carton et al., 2018) where the ESA-CCI product is not available. Silicate and phosphate concentrations were taken from the World Ocean Atlas 2018 (Boyer et al., 2018).

Following many previous studies (e.g., Lauvset et al., 2015; Bates et al., 2014), we use here the total scale for pH, which includes the contribution of sulfate ions (A. G. Dickson, 1993). In contrast, we report for $[H^+]$ its free concentration, which is equivalent to pH on the free scale (Clayton & Byrne, 1993), i.e., without the contribution of the sul-

fate ions. We use the saturation state of Ω_{ar} as the second metric to quantify the evolution of OA (Mucci et al., 1983; Takahashi et al., 2014). Although aragonite is ∼50% more soluble than calcite, the trends for its two saturation states tend to be nearly identical.

Trends are calculated on annual averages using an ordinary least squares (OLS) regression. We thereby determined the uncertainties of the trends based on the two-sided inverse Students t-distribution for a 95% confidence interval with $(n-2)$ degree of freedom, where n is the number of data in the global mean time series. The uncertainties of the global mean trends are then computed by multiplying the critical value of the t-distribution with the standard errors of the estimate for the slopes. The reported uncertainty thus reflects only the uncertainty of the trend and thus does not include any error in the underlying data.

2.2 Driver decomposition of trends

We decompose the trends in Ω_{ar} and $[H^+]$ into contributions from trends in the main drivers, that is DIC, Alk, T and freshwater (FW). The freshwater driver includes both the direct effect of changes in salinity on Ω_{ar} and pH, as well as the indirect effect caused by changes in the surface ocean DIC and Alk due to the net freshwater balance (Lovenduski et al., 2007; Landschützer et al., 2018). To this end, we remove the freshwater component from the DIC and Alk driver by normalizing these two parameters to a constant salinity of 34.5 (Sarmiento & Gruber, 2006; Landschützer et al., 2018). The resulting quantities are denoted by sDIC and sAlk. We further decompose DIC into an anthropogenic and a natural component, DIC = $C_{ant} + C_{nat}$, i.e., the component driven solely by the anthropogenic increase in atmospheric CO_2 and the resulting uptake of anthropogenic CO_2 by the surface ocean, and the component driven by changes in circulation and biology (McNeil & Matear, 2013; Gruber et al., 2023).

Neglecting the contributions from other minor drivers such as nutrients, we thus decompose the variations in the trends of Ω_{ar} and $[H^+]$ to five main driving components: anthropogenic sDIC (C_{ant}), natural sDIC (C_{nat}), sAlk (A), temperature (T) and freshwater (FW). Considering only the first-order terms of a Taylor expansion and using the product rule, this gives the rate of change of Ω_{ar}:

$$\frac{d\Omega_{ar}}{dt} = \sum_{X=[C_{ant},C_{nat},A,T,FW]} \left(\underbrace{\frac{d\omega_X}{dt} \cdot \Omega_{ar} \cdot \Delta X}_{\text{change in sensitivity}} + \underbrace{\omega_X \cdot \frac{d\Omega_{ar}}{dt} \cdot \Delta X}_{\text{mass effect}} + \underbrace{\omega_X \cdot \Omega_{ar} \cdot \frac{d\Delta X}{dt}}_{\text{change in driver}} \right), \tag{2}$$

where X is one of the five drivers, ΔX is the change in the driver (from 1982 through 2021), and ω_X is the relative sensitivity of Ω_{ar} to each driver, i.e., $\omega_X = 1/\Omega_{ar} \cdot \partial\Omega_{ar}/\partial X$. Note that this definition of ω_X differs from that of Egleston et al. (2010) who defined it as the sensitivity of X to Ω_{ar}. The time derivatives on the right-hand side of (2) are determined from the slopes of the linear regressions.

The same decomposition is applied for $[H^+]$, i.e.,

$$\frac{d[H^+]}{dt} = \sum_{X=[C_{ant},C_{nat},A,T,FW]} \left(\underbrace{\frac{d\beta_X}{dt} \cdot [H^+] \cdot \Delta X}_{\text{change in sensitivity}} + \underbrace{\omega_X \cdot \frac{d[H^+]}{dt} \cdot \Delta X}_{\text{mass effect}} + \underbrace{\omega_X \cdot [H^+] \cdot \frac{d\Delta X}{dt}}_{\text{change in driver}} \right), \tag{3}$$

where β_X is the relative sensitivity of [H$^+$] to each driver X, i.e., $\beta_X = 1/[H^+] \cdot \partial[H^+]/\partial X$. The relative sensitivities β and ω are calculated with the PyCO2SYS program (Lewis et al., 1998; Humphreys et al., 2020) for each grid point, using the long-term average conditions as input. The temperature sensitivities are assumed to be constant for the entire range of DIC and Alk, with a value of 0.0052 °C^{-1} for Ω_{ar} and a value of 0.0354 °C^{-1} for [H$^+$].

The surface ocean concentration of C_{ant} and its rate of change is estimated by assuming that surface ocean DIC increases proportionally with the increase in atmospheric CO_2 (Gruber et al., 2023). We determine this proportionality by computing first the amount of C_{ant} the surface ocean would have if it had remained in transient equilibrium with the overlying atmosphere, i.e., the C_{ant}^{eq} component. We then adjust this component to account for the fact that the increase in surface C_{ant} is increasingly delayed, leading to a growing disequilibrium term, i.e., C_{ant}^{dis-eq}, which is also proportional to the rise in atmospheric CO_2 (see Matsumoto and Gruber (2005) for a more in-depth discussion). Concretely, C_{ant} is given by: $C_{ant} = C_{ant}^{eq}$ - C_{ant}^{dis-eq}. We determine C_{ant}^{eq} at each surface location by evaluating (1) whereby the in situ pCO_2 is replaced with atmospheric CO_2 from the NOAA marine boundary layer product (Dlugokencky et al., 2021). We take the disequilibrium term C_{ant}^{dis-eq} from a hindcast simulation with the ocean component of the Community Earth System Model (CESM) (Clement & Gruber, 2018; Hauck et al., 2020). The trend in the natural component, C_{nat}, is computed by subtracting C_{ant} from sDIC, i.e., C_{nat} = sDIC - C_{ant}, whereby all components are salinity normalised to 34.5.

2.3 Time of Emergence

The Time of emergence (ToE) is defined as the time it takes for a signal to arise from the noise of natural climate variability (Keller et al., 2014):

$$\text{ToE} = (2 \times \text{N})/\text{S} \tag{4}$$

where N is the standard deviation of the detrended and deseasonalized monthly data, and S is the annual trend. This results in TOE having an output in units of years.

3 Results and Discussions

3.1 Evaluation

The rate of pH change estimated from OceanSODA-ETHZ generally agrees well with the reported rates from observation stations around the globe (Table S1 in the supplementary material). However, many stations have reported trends over much shorter periods, making the comparisons less robust owing to a stronger imprint of interannual variability. We thus focus the evaluation of our trend estimates with those stemming from the longest-running (> 30 years) and best-sampled time series sites in the ocean, namely the Hawaii Ocean Time-series (HOT) (Dore et al., 2009) in the North Pacific, the Bermuda Atlantic Time series Study (BATS) in the North Atlantic (Bates et al., 2014; Bates & Johnson, 2020) (Table S2). This evaluation is particularly insightful since the data from these two time series sites were not used for the training of the machine-learning algorithm in OceanSODA-ETHZ. Neither site measured pH or Ω_{ar}, but DIC and Alk, from which we computed pH and Ω_{ar} following the same procedures as for OceanSODA-ETHZ. We also recomputed the long-term trends in order to ensure maximum comparability with our estimates. To this end, we first deseasonalized the data from the time series stations using a harmonic fit (Gruber et al., 2002) and then computed the trend in the same manner as done for OceanSODA-ETHZ.

For BATS and the period covered by this site, i.e., 1992-2021, we compute for OceanSODA-ETHZ a decadal rate of change for pH of -0.017±0.001 decade^{-1}, numerically identical to what we determined from the reported time series data. By including data from the

nearby Station "S" (Gruber et al., 2002), Bates and Johnson (2020) was able to extend this record back in time, reporting for 1983-2020 a slightly more negative trend of -0.019±0.001 decade^{-1} (Table S1), a bit more negative than our estimate for the same period (-0.016±0.001), but still within the uncertainties. The trends for Ω_{ar} are slightly more different, but still in agreement. While our estimate for the period 1992-2021 of -0.061±0.005 decade^{-1} is again numerically identical to that we computed from the time series data, Bates and Johnson (2020) found for the combined Station "S" and BATS sites over the 1983-2020 period a trend of -0.09±0.01 decade^{-1}, which is quite a bit more negative than ours (Table S1).

Our pH trend estimate for the HOT site (1989-2021) of -0.018±0.001 decade^{-1} is again the same as that we computed from the reported time series data (-0.018±0.001 decade^{-1}). But, as was the case at BATS, there is a somewhat less agreement on the trend in Ω_{ar}. For OceanSODA-ETHZ, we find a trend of -0.083±0.005 decade^{-1}, while for the time series data, the trend amounts to -0.089±0.006 decade^{-1}.

The evaluation of the trends at the other time series sites (Table S1 in the supplementary material), often of much shorter duration, confirms the overall excellent agreement. But this comparison also suggests that the OceanSODA-ETHZ has a slight tendency for underestimating long-term trends, especially for Ω_{ar}. This could be a consequence of the cluster-regression approach that we employed in ensemble mode to create OceanSODA-ETHZ, as this machine-learning method tends to suppress variations and trends (Gregor & Gruber, 2021). Still, these evaluations suggest that OceanSODA-ETHZ reproduces the observed long-term trends at the time series stations with high fidelity, giving us confidence in the use of this product to assess long-term trends in OA across the global ocean (Chau et al., 2022).

3.2 Long-term trends

The temporal evolution of the reconstructed global surface mean Ω_{ar}, pH, and $[H^+]$ from the OceanSODA-ETHZ product confirm the expected strong trends induced by ocean acidification over the four decades from 1982 through 2021 (Fig. 1). Averaged over the global ice-free ocean, surface Ω_{ar} decreased by nearly 10% over these four decades, and pH experienced a drop of ∼0.06 units. At the same time, $[H^+]$ increased proportionately by slightly more than 1 nmol kg^{-1}. This translates into highly significant average trends of -0.071 ± 0.001 decade^{-1} for Ω_{ar} ($R^2 = 0.98$; $p \ll 0.01$) and -0.0170 ± 0.0001 decade^{-1} for pH ($R^2 = 0.99$; $p \ll 0.01$). For $[H^+]$ the average rate of increase amounts to 0.240 ± 0.004 nmol kg^{-1} decade^{-1}. The global trends are very insensitive to the choice of the exact beginning or ending years. For example, shortening the record to 30 years and computing the trends by shifting the beginning year from 1982 to 1992 yields variations in the trends of $< 7\%$.

The reported uncertainties of the trends reflect just the statistical uncertainty of the regression slope, and thus do not include any additional uncertainties induced by systematic errors associated with the underlying data. In order to obtain a zeroth order estimate of this contribution, we determined the trends for each individual ensemble member in the OceanSODA-ETHZ product and computed the resulting standard deviation. This resulted in essentially the same uncertainty as the reported trend uncertainty. Larger contributions to the trend uncertainty could stem from biases in our mapped product that change with time, such as those that could be induced from changed sampling through time, or from temporally changing systematic errors in the measurements of pCO_2 and/or alkalinity that underlie the OceanSODA-ETHZ product. Although we have not found any indication of such temporally changing errors (Gregor & Gruber, 2021), we cannot exclude this either. We thus conclude that the reported trend uncertainties are likely an underestimate, perhaps by several fold. Even if we adopted, for example, a fivefold increase in the uncertainty, the relative uncertainties of the trend estimates would remain

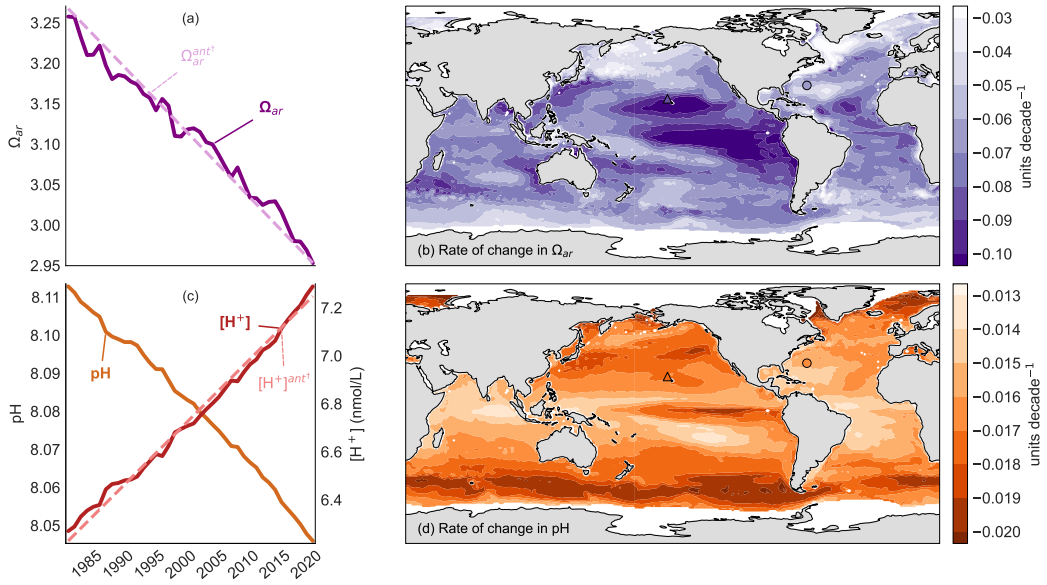

Figure 1. Temporal and spatial structure of the long-term trends in global aragonite saturation state (Ω_{ar}), pH, and [H^+] from 1982 to 2021 using OceanSODA-ETHZ data (Gregor & Gruber, 2021). (a) Global area-weighted trend for Ω_{ar} (solid line), along with the estimated anthropogenic trend (dashed line) based on the increase in C_{ant}. (b) Global map of the 40-year average trend of Ω_{ar}, expressed as trend per decade. (c) As (a) but for pH (left axis) and [H^+] (right axis) with the estimated anthropogenic increase being shown for the latter only. (d) As (b), but for pH. Note that the global average trends plotted in (a) and (c) are computed over the colored areas shown in (b) and (d), representing 96% of the global sea-ice-free surface area. The triangle and circle in (b) and (d) indicate the locations of the two time series HOT and BATS used to evaluate the OceanSODA-ETHZ product in detail.

at less than 10%. We consider this an extremely pessimistic case, but we lack information to provide a better estimate of the true uncertainty.

Our global mean surface pH trend supports the trend estimated by Lauvset et al. (2015) of 0.018±0.004 for the period 1991 through 2011, we can now provide a much more accurate estimate covering 96% of the global sea-ice-free surface ocean as opposed to the 70% coverage available to Lauvset et al. (2015). Even when considering our potential underestimation of the trend uncertainty, our estimate permits us also to reduce the range given by IPCC (Bindoff et al., 2019), i.e., -0.017 to -0.027 decade^{-1}, by more than tenfold. Our global pH trend matches also well those given by a range of Earth System Models (Kwiatkowski et al., 2020). Unfortunately, we are unaware of reported global ocean mean trends for Ω_{ar}.

Spatially, the rates of the Ω_{ar} and pH declines over the past four decades vary substantially across the open ocean (Fig. 1b,d)(see also Suppl. Tables S3 and S4). For Ω_{ar}, the largest trends are found in the tropical and subtropical Pacific Ocean, including the eastern tropical Pacific region (Fig. 1b), with rates of Ω_{ar} decreases that are, on average, 50% higher than in the global mean. In contrast, Ω_{ar} drops much less in the North Pacific and North Atlantic and parts of the Southern Ocean. Here, rates tend to be only half those of the global mean. This gives overall a factor of four difference in rates across the global ocean, highlighting the importance of the regional perspective when investigating ocean acidification.

The spatial distribution of the decline in pH tends to be the mirror image of that of Ω_{ar} (Fig. 1d), although the range is smaller. The highest rates of decline are found in the Southern Ocean and in the high latitudes of the North Atlantic and North Pacific. Rates are here, expressed in the logarithmic pH units, about 15% higher than in the global mean. The lowest rates of changes are found in the subtropical gyres, with rates that are about 25% lower than the global mean. Another striking pattern is that the trends in the Pacific tend to be larger than those in the Pacific for the same latitude. A region that breaks the mirror image, i.e., where both Ω_{ar} and pH show large changes, is a small equatorial band in the eastern and central Pacific.

The distinct spatial variations of the rates of change of ocean acidification had been discussed in the literature only sparingly so far. Lauvset et al. (2015) also found trends that varied considerably across the analyzed biomes, but given the large uncertainties of their regional trends, they refrained from discussing them in detail. They did point to the systematic differences between the Atlantic and Pacific, however. A systematic difference we can confirm here. In its global assessment, IPCC AR6 (Canadell et al., 2021) discussed the regional differences as well, pointing out, for example, that the central and eastern upwelling zones of the Pacific exhibited a faster pH decline of –0.022 to –0.026 decade^{-1} (see also Sutton et al. (2014)) compared to the western tropical Pacific, where the trends are only in the range of –0.010 to –0.013 decade^{-1} (see also Ishii et al. (2020)). This strong east-west gradient in the tropical Pacific is fully confirmed by our results (Fig. 1d). IPCC AR6 further suggested for the subtropical gyres pH trends ranging from -0.016 to -0.019 decade^{-1}, which is a smaller range than that we find (-0.013 to -0.019 decade^{-1}). In contrast, IPCC AR6 suggests subpolar latitudes values ranging from -0.003 decade^{-1} to -0.026 decade^{-1}, while our work suggests a substantially smaller range (-0.017 to -0.020 decade^{-1}). We interpret these differences to be primarily the result of the relatively small number of time series sites that were used by the IPCC for their assessment. We are not aware of any study that investigated the spatial pattern of the trend in Ω_{ar} in a systematic manner, although IPCC AR6 (Canadell et al., 2021) mentioned the regional differences.

3.3 Drivers of the long-term trends

The driver decomposition (2) & (3) confirms the expectation that the majority of the decreasing trend in Ω_{ar} and increasing trend in $[H^+]$ is driven by the anthropogenic increase in atmospheric pCO_2 causing an increase in surface ocean C_{ant} (dashed lines in Fig. 1a,c). This conclusion is in line with IPCC's assessments (Canadell et al., 2021; Bindoff et al., 2019) as well as with prior work (Lauvset & Gruber, 2014; Lauvset et al., 2015). However, hidden behind the dominating role of C_{ant} are substantial and relevant contributions from the other drivers. A first indication of this comes from the global trend in Ω_{ar} in Fig. 1a), which is decreasing substantially less rapidly than expected from the anthropogenic trend alone. This differs markedly from the trends in pH and $[H^+]$, which agree remarkably well with the anthropogenic trend. A second indication comes from the full driver decomposition in Fig. 2a,b, which show that changes in natural CO_2, temperature, and to a somewhat smaller degree also sAlk, contribute substantially to the trends, especially for $[H^+]$. We discuss these two indications in sequence.

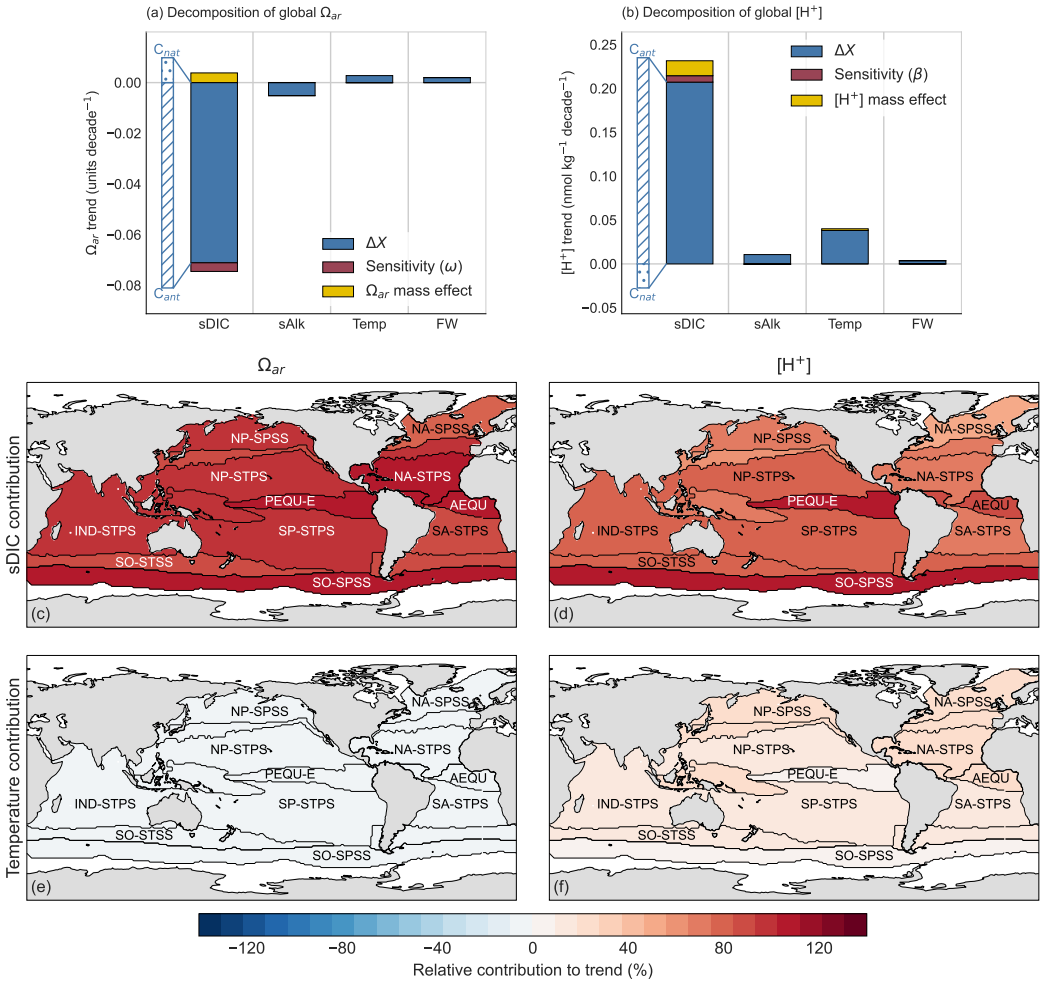

Figure 2. Decomposition of the global mean rate of change of (a) Ω_{ar} and (b) [H$^+$] over the period 1982-2021 into their main drivers following equations (2) & (3) in the main text. The considered drivers are: salinity normalized dissolved inorganic carbon (sDIC) separated into its anthropogenic CO2 (C_{ant}) and natural CO2 (C_{nat}) components, sea surface temperature (SST), salinity normalized alkalinity (sAlk), and freshwater (FW). Also shown for each driver are the contribution of the three mechanisms: change in the driver sensitivity (blue), change in the carbonate system variable (yellow), and change in the driver itself (red). Also shown here are maps showing the relative contribution of (c) sDIC to the rate of change of Ω_{ar}, (d) sDIC to the trend of $[H^+]$, (e) SST to the trend in Ω_{ar}, and (f) SST to the trend in $[H^+]$ aggregated to each biome.

According to our decomposition, the main reason for the smaller than expected long-term trend in Ω_{ar} is the substantial compensation by natural CO2 (C_{nat}) (Fig. 2a). This means that in the OceanSODA-ETHZ product, the concentration of sDIC is not increasing as fast as predicted from the increase in anthropogenic CO2 (C_{ant}) because of a loss in C_{nat}. Since changes in sAlk are relatively minor and even suggesting a small increase, this smaller than expected increase in sDIC causes a lower rate of decrease of the carbonate ion concentration predicted from the increase in C_{ant} alone, hence causing a lower rate of decrease of Ω_{ar}. Also warming and the freshwater component actually act to compensate for the anthropogenic CO2 driven decrease in Ω_{ar}, but their contribution is small (Fig. 2a). Similarly, the mass effect slows the rate of decrease of Ω_{ar}. In summary, the

contribution of the non-sDIC components is small, so that it is the decrease in C_{nat}, i.e., the reduction in the concentration of natural CO_2 in the surface ocean, that causes global mean Ω_{ar} to decrease less rapidly than predicted from the rise in atmospheric CO_2 alone.

The decomposition of the trends for $[H^+]$ reveals a different picture (Fig. 2b). While the strong increase in $[H^+]$ driven by C_{ant} is also compensated by the decrease in C_{nat}, the other components, are contributing substantially to the driving up of the trend in $[H^+]$ (Fig. 2b). The most important driver is temperature, which contributes $\sim$ 15% to the rate of increase in $[H^+]$. But also the $[H^+]$ mass effect and the increased sensitivity contribute to the rise in $[H^+]$. Taken together, a different balance emerges for the trend in $[H^+]$ compared to that of Ω_{ar}. For $[H^+]$, the slowing trend induced by the loss of C_{nat} is nearly entirely compensated for by the accelerating trend induced by surface ocean warming, so that the overall trend is remarkably close to that predicted by C_{ant} alone. In other words, the loss of C_{nat} tends to mask the quite substantial accelerating contribution of ocean warming on the trend of $[H^+]$.

Thus for both trends, we find an important modification of the purely anthropogenic CO_2 trend by surface ocean warming and the loss of C_{nat}, albeit with different relative roles. Before we discuss this finding further, we need to ensure that it is robust. This is especially critical since we estimate the trend in C_{nat} by difference from the trend in sDIC and C_{ant}. Of particular concern is our estimate of the disequilibrium component, which we use to adjust the equilibrium estimate of C_{ant} for the fact that even in the absence of any climate variability surface ocean sDIC is not following perfectly the increase in atmospheric CO_2 owing to the slowness of air-sea gas exchange and limited surface residence times (Matsumoto & Gruber, 2005). Globally, the mean air-sea disequilibrium is actually very well-constrained since it is directly related to the oceanic uptake of anthropogenic CO_2, which is known to within about $\pm$15% on the basis of multiple approaches (Gruber et al., 2023, 2019; Hauck et al., 2020; DeVries, 2014; Mikaloff Fletcher et al., 2006; Sabine et al., 2004). It turns out that even adopting an uncertainty for the air-sea disequilibrium of C_{ant} of $\pm$30% would not alter our conclusion that C_{nat} has decreased over the last four decades. We thus consider this conclusion as robust.

The diagnosed loss of C_{nat} from the surface ocean slowing down the rate of change of Ω_{ar} and $[H^+]$ can also be rationalized from a process perspective, especially since it is connected to surface ocean warming. First, one expects a loss of C_{nat} form the surface ocean in response to the reduced CO_2 solubility associated with surface warming (Weiss, 1974). Second, upper ocean warming has been linked to the observed increase in upper ocean stratification (Sallée et al., 2021), which tends to make the biological pump more efficient, causing a reduction in surface ocean DIC (Sarmiento & Gruber, 2006).

The important contribution of ocean warming to the long-term trend in $[H^+]$ becomes also very clear when investigating this decomposition on a regional basis, here shown just for the contribution from sDIC, i.e., the sum of natural and anthropogenic CO_2 (Fig. 2c-d), and for temperature (Fig. 2e-f). While the contribution of warming to the trend in Ω_{ar} is less than a few percent, this number is about 8% for $[H^+]$, on average. The highest contributions are found in the North Atlantic and the western Pacific, i.e., the regions that experienced the highest rates of surface warming in the last few decades (Johnson & Lyman, 2020).

Still, the majority of the long-term trend for both $[H^+]$ and Ω_{ar} across all regions stem from the increase in sDIC (Fig 2c-d). This means that the distinct spatial differences in the rates of change in $[H^+]$ and Ω_{ar} seen in Fig. 1 and shown as zonal means in Fig 3.3c,f are caused by the product of the spatial pattern of the sensitivities β_{DIC} and ω_{DIC}, respectively with the trend in C_{ant} (see Fig. supplementary S5), whose spatial pattern is given by the inverse of the sensitivity γ_{DIC} (Egleston et al., 2010). This means that one can understand the trends in $[H^+]$ and Ω_{ar} as being proportional to the ratio of β_{DIC}/γ_{DIC} and $\omega_{DIC}/\gamma_{DIC}$, respectively (see also Orr (2011) for a detailed dis-

cussion). All of these sensitivities are reflections of how well the surface carbonate chemistry is able to buffer the increase in surface ocean CO_2, which depends on temperature, and especially the ratio of DIC and Alk (Sarmiento & Gruber, 2006; Egleston et al., 2010).

In the case of the trends in $[H^+]$ (and pH), the high sensitivity of β_{DIC} at the high latitudes (Figure S4), largely driven by temperature, overwhelms the impact of the higher rates of change in C_{ant} in the low latitudes owing to higher buffer capacities (Sabine et al., 2004) (or lower γ_{DIC}), such that the highest rates of changes in $[H^+]$ (pH) are found in the high latitudes. For Ω_{ar}, the situation is reversed. Here the high buffer capacity of the low latitudes (small γ_{DIC}) with the corresponding higher rates of accumulation of C_{ant} overwhelms the effect of ω_{DIC}, which has the highest (absolute) sensitivity in the high latitudes as well. The net result is that the highest rates of change in Ω_{ar} occur in the low latitudes. This also means that the highest decreases in Ω_{ar} occur in the regions where Ω_{ar} is highest, while for $[H^+]$, the highest increases occur where $[H^+]$ is already high, i.e., where pH is lowest (Fig 3.3a,d). The former can be largely understood from the fact that the highest rates with which $[CO_3^{2-}]$ is titrated away from the invasion of C_{ant} through the short-circuit reaction $CO_2 + CO_3^{2-} + H_2O = 2HCO_3^-$ (Sarmiento & Gruber, 2006) occurs in the regions where $[CO_3^{2-}]$ is most abundant, i.e. where Ω_{ar} is highest. The latter is directly the inverse, i.e., the regions where most of the invading C_{ant} is not titrated away but rather stay in its acid form through reaction with water to form H_2CO_3 is where $[CO_3^{2-}]$ (and hence also Ω_{ar}) is the lowest, and where $[H^+]$ is highest (or pH lowest).

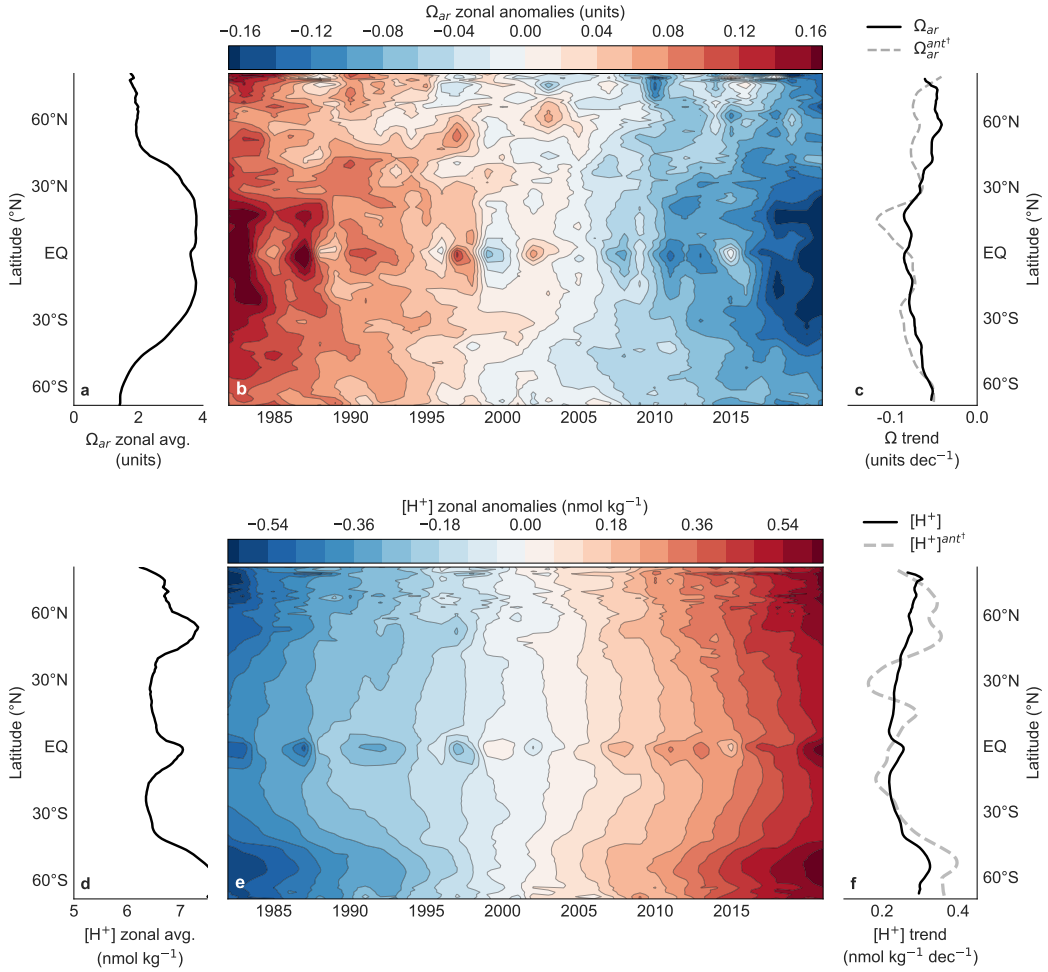

Figure 3. Hovmoeller (latitude-time) diagrams of the zonally averaged anomalies from 1982 to 2021 together with their long-term averages and zonal mean trends. (a) Zonal average of the long-term mean Ω_{ar}. (b) Hovmoeller diagram of the zonally averaged anomalies of Ω_{ar}. The anomalies have been computed relative to the long-term mean shown in (a). (c) Zonal average of the long-term linear trend in Ω_{ar} (solid line) together with the trend estimated solely on the basis of the estimated increase in anthropogenic CO2 (dashed line). (d) As (a), but for $[H^+]$. (e), as (b) but for $[H^+]$. (f), as (c) but for $[H^+]$.

3.4 Interannual Variability

In addition to the long-term trends, both Ω_{ar} and $[H^+]$ are subject to a substantial amount of interannual variability Fig. 3.3, with Ω_{ar} revealing a much more variable pattern than $[H^+]$. The interannual variability for $[H^+]$ is primarily confined to the equator, with distinct negative $[H^+]$ anomalies found around 1983, 1987, 1992, 1998, 2002, etc., i.e., years characterized by El Niño events in the tropical eastern Pacific. These negative $[H^+]$ anomalies are likely caused by the near cessation of upwelling during these events, thus bringing much less high DIC/low Alk (low $[H^+]$) waters to the surface, keeping surface $[H^+]$ low (and pH high). Even though these events are also characterized by higher than normal sea-surface temperatures, this effect appears to be overwhelmed by the low DIC concentrations that characterize El Niño events (McKinley et al., 2004; R. Feely et al., 2006). Positive anomalies in $[H^+]$ occur during La Niña events, when upwelling

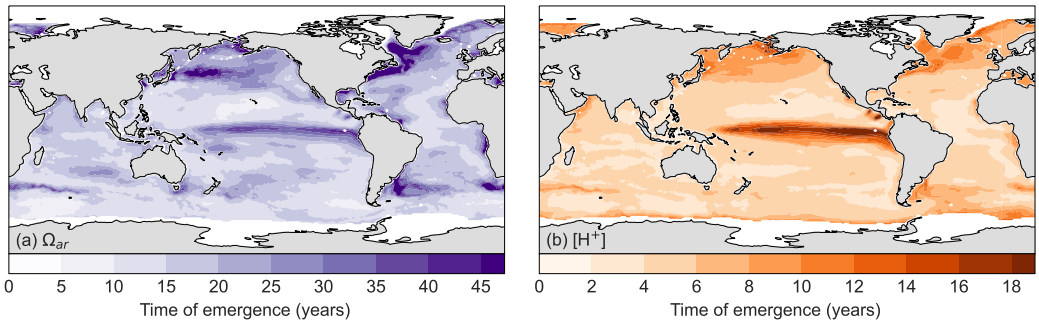

Figure 4. Maps depicting the time of emergence (ToE) for (a) Ω_{ar} and (b) pH. The ToE was estimated from the rates of change in Ω_{ar} and pH and variations in their respective deseasonalized monthly data, see eq(4) in the main text.

is strong, bringing large amounts of high DIC/low Alk waters to the surface(Sutton et al., 2014).

The Ω_{ar} anomalies at equatorial latitudes are the opposite of those of $[H^+]$, i.e., Ω_{ar} tends to be anomalously high during El Niño events and anomalously low during La Niña events. The drivers are the same as those for $[H^+]$, i.e., variations in the strength of upwelling that tends to bring high DIC/low Alk (low Ω_{ar}) waters to the surface.

The Hovmoeller plot for Ω_{ar} reveals also a substantial amount of interannual variability in the extratropics, especially when compared to $[H^+]$ (contrast Fig. 3.3b with panel f). The variability in the zonal mean comes from all ocean basins. It is most likely related to the interaction of transport/mixing and biological production that tend to change Ω_{ar} in opposite direction. Their effect is not dampened by co-variations with temperature, since temperature plays a relatively marginal role in controlling Ω_{ar}. This situation tends to differ for $[H^+]$, where surface warming/cooling often dampens the effects of transport/mixing and biological production, leading to a lower level of variability (see also Jiang et al. (2019)).

3.5 Time of Emergence

Across the global ocean, the times of emergence (ToE) for both Ω_{ar} and pH estimated from OceanSODA-ETHZ are on the scale of years to decades (Fig. 4), but with large regional differences between the two parameters. The ToE of Ω_{ar} ranges from a value of near 1 year up to nearly 50 years while that of pH ranges from near 1 year to around 20 years only. However, for the majority of the open oceans, ToE of both Ω_{ar} and pH is on the time scales of a few years to a decade. Ω_{ar} exhibits generally longer ToE than pH in most locations, especially in the Northern Hemisphere, largely caused by the higher level of variability in Ω_{ar} shown in Fig. 3.3. For both Ω_{ar} and pH, the eastern equatorial Pacific is estimated to have one of the longest ToE (decade to several decades), since this is the region where both parameters vary interannually the most. For Ω_{ar}, ToE is also long in the mid to high-latitude oceans, including the high-latitude north Pacific, north Atlantic, and south Atlantic.

These findings imply that at most within half a century, the underlying trends in Ω_{ar} and $[H^+]$ will become strong enough to exceed their interannual variability for most of the open oceans. Correlation between the ToE distributions of these two OA parameters also indicates that the development of acidification can be easily detected amidst interannual variations in a time frame of a few decades for vast regions of the global oceans.

Our estimate of the ToE compares well with those that have been estimated from models so far (Schlunegger et al., 2019; Rodgers et al., 2015; Keller et al., 2014; Friedrich et al., 2012), although differences in the definition make direct quantifications difficult. For example, Friedrich et al. (2012) used the amplitude of the seasonal cycle as the metric of variance, whereas we use here the standard deviation of the deseasonalized data, i.e., we consider primarily the level of interannual variability as the "noise" against which we aim to detect the signal. Schlunegger et al. (2019) and Rodgers et al. (2015) used the "noise" from an ensemble of models and compared that to the trend emerging from the ensemble mean, which is closer to our definition, but still different. Despite these important differences, our work here confirms prior assessments that the signals from ocean acidification emerge relatively fast, i.e., on the order of years to decades, from the background noise. Our results also confirm prior findings that the equatorial Pacific has one of the longest ToEs(Rodgers et al., 2015). Previously not discussed was the difference between pH and Ω_{ar}, which we are now able to show.

3.6 Caveats and limitations

We note that the interannual variability of pH, $[H^+]$, and Ω_{ar} in the OceanSODA-ETHZ product may be underestimated. We base this potential caveat on the observation that the variability of the pCO_2 data in OceanSODA-ETHZ is on the low end compared to that exhibited in six other surface ocean pCO_2 products (Table S5 in supplementary). Comparison of zonally averaged interannual variability of pCO_2 between the OceanSODA-ETHZ data set (lowest interannual variability of the seven products) and six other pCO_2-products suggests that the largest discrepancy in their respective interannual variability estimates exists in the high latitudes (Fig. S6 in supplementary). A systematically low interannual variability in the OceanSODA-ETHZ product would directly lead to a systematic underestimation of the ToE. Thus, we conclude that our ToE results may be biased low, although we suspect that this systematic underestimation of the variability would not alter the regional differences.

In addition, we also note that our driver decomposition could be biased since we use the same variables as predictors for generating the fields in the first place and for diagnosing the decomposition in the second place. This is potentially problematic since the predictors are interdependent, especially SST and SSS. While this may not cause problems when predicting the distribution of the variables, it may be problematic when diagnosing the role of freshwater forcing and heating/cooling of the sea surface. We currently do not know how to address this, but we also do not have any evidence that this is an issue. Still, one needs to be aware of this potential caveat when analyzing the driver decomposition.

4 Summary and Conclusions

Our analyses of the OceanSODA-ETHZ product suggest that global surface ocean Ω_{ar} and pH have declined over the past 4 decades at rates of -0.071 $\pm$ 0.001 and -0.0170 $\pm$ 0.0001 units per decade, respectively. Both trends are predominantly caused by the increase in atmospheric CO_2 driving a trend in the surface ocean concentration of anthropogenic CO_2. But we also showed that a decrease in the surface ocean concentration of natural CO_2 and ocean warming modulate the trends measurably. Especially noteworthy is the $\sim$15% enhancement of the pH trend by ocean warming. ENSO dominates the interannual variability in both Ω_{ar} and pH, although Ω_{ar} has greater interannual variability. This leads to a substantially longer time of emergence for Ω_{ar} (several decades) compared to pH (around a decade).

Our global trend analyses represent a major step forward relative to prior data-based assessments of the global trends in OA, which were either based on a limited number of time series stations (Canadell et al., 2021) or based on spatial aggregation of data

over large-scale biomes (Lauvset et al., 2015). Not only were we able to substantially reduce the uncertainties of the trends, but we also pointed out the substantial regional differences in the trends of the most important OA parameters with pH experiencing, on average, the highest rates of changes in the higher latitudes, while the largest changes in Ω_{ar} are found in the tropics. These regional differences need to be taken into account when assessing the impact of OA across the global surface ocean. For example, the especially high rates of change in Ω_{ar} in the eastern Pacific can bring warm-water corals in toward critical saturation thresholds (Hoegh-Guldberg et al., 2007) much faster than inferred from the globally averaged rate of change of Ω_{ar}. Our observation-based analyses can provide also important evaluation constraints for model studies used to project OA into the future (Kwiatkowski et al., 2020). Of particular concern is again the spatial structure of the simulated changes, an aspect that has not been given a lot of attention so far.

Understanding the long-term trends and variability of global acidification enables us to put local changes into the larger context of global trends and variability. Even though we emphasized here the role of other drivers, the main driver of OA is the increase in atmospheric CO_2. Thus, unless the anthropogenic emissions of CO_2 are massively curtailed, OA is bound to continue, increasing its threats on marine life (Kroeker et al., 2013; Bindoff et al., 2019).

Acknowledgments

This research has been supported by the European Space Agency (OceanSODA project, grant no. 4000112091/14/I-LG), and by the European Commission through its Horizon 2020 research and innovation programme under grant agreements no. 821003 (project 4C) and no. 820989 (COMFORT).

References

Bates, N. R. (2007). Interannual variability of the oceanic CO_2 sink in the subtropical gyre of the North Atlantic Ocean over the last 2 decades. *Journal of Geophysical Research: Oceans*, *112*(C9).

Bates, N. R., Astor, Y. M., Church, M. J., Currie, K., Dore, J. E., González-Dávila, M., ... Santana-Casiano, J. M. (2014). A time-series view of changing surface ocean chemistry due to ocean uptake of anthropogenic CO_2 and ocean acidification. *Oceanography*, *27*(1), 126–141.

Bates, N. R., & Johnson, R. J. (2020). Acceleration of ocean warming, salinification, deoxygenation and acidification in the surface subtropical north atlantic ocean. *Communications Earth & Environment*, *1*(1), 33.

Bindoff, N. L., Cheung, W. W., Kairo, J. G., Arístegui, J., Guinder, V. A., Hallberg, R., ... others (2019). Changing ocean, marine ecosystems, and dependent communities. *IPCC special report on the ocean and cryosphere in a changing climate*, 477–587.

Bopp, L., Resplandy, L., Orr, J. C., Doney, S. C., Dunne, J. P., Gehlen, M., ... others (2013). Multiple stressors of ocean ecosystems in the 21st century: projections with CMIP5 models. *Biogeosciences*, *10*(10), 6225–6245.

Boutin, J., Vergely, J.-L., Marchand, S., d'Amico, F., Hasson, A., Kolodziejczyk, N., ... Vialard, J. (2018). New smos sea surface salinity with reduced systematic errors and improved variability. *Remote Sensing of Environment*, *214*, 115–134.

Boyer, T. P., Garcia, H. E., Locarnini, R. A., Zweng, M. M., Mishonov, A. V., Reagan, J. R., ... Smolyar, I. V. (2018). World Ocean Atlas 2018. *NOAA National Centers for Environmental Information*.

Brewer, P. G. (2013). A short history of ocean acidification science in the 20th cen-

tury: a chemist's view. *Biogeosciences*, *10*(11), 7411–7422.

Byrne, R. H., & Breland, J. A. (1989). High precision multiwavelength pH determinations in seawater using cresol red. *Deep Sea Research Part A. Oceanographic Research Papers*, *36*(5), 803–810.

Caldeira, K., & Wickett, M. E. (2003). Anthropogenic carbon and ocean ph. *Nature*, *425*(6956), 365–365. Retrieved from `https://doi.org/10.1038/425365a` doi: 10.1038/425365a

Canadell, J. G., Monteiro, P. M., Costa, M. H., Da Cunha, L. C., Cox, P. M., Alexey, V., ... others (2021). *Global carbon and other biogeochemical cycles and feedbacks.*

Carton, J. A., Chepurin, G. A., & Chen, L. (2018). SODA3: A new ocean climate reanalysis. *Journal of Climate*, *31*(17), 6967–6983.

Chau, T. T. T., Gehlen, M., & Chevallier, F. (2022). A seamless ensemble-based reconstruction of surface ocean pCO_2 and air–sea CO_2 fluxes over the global coastal and open oceans. *Biogeosciences*, *19*(4), 1087–1109.

Claustre, H., Johnson, K. S., & Takeshita, Y. (2020). Observing the global ocean with biogeochemical-argo. *Annual review of Marine science*, *12*, 23–48.

Clayton, T. D., & Byrne, R. H. (1993). Spectrophotometric seawater pH measurements: total hydrogen ion concentration scale calibration of m-cresol purple and at-sea results. *Deep Sea Research Part I: Oceanographic Research Papers*, *40*(10), 2115–2129.

Clement, D., & Gruber, N. (2018). The eMLR(C*) method to determine decadal changes in the global ocean storage of anthropogenic CO_2. *Global Biogeochemical Cycles*, *32*(4), 654–679. Retrieved from `http://doi.wiley.com/10.1002/2017GB005819https://onlinelibrary.wiley.com/doi/10.1002/2017GB005819` doi: 10.1002/2017GB005819

Cornwall, C. E., Comeau, S., Kornder, N. A., Perry, C. T., van Hooidonk, R., DeCarlo, T. M., ... others (2021). Global declines in coral reef calcium carbonate production under ocean acidification and warming. *Proceedings of the National Academy of Sciences*, *118*(21).

Cornwall, C. E., Harvey, B. P., Comeau, S., Cornwall, D. L., Hall-Spencer, J. M., Peña, V., ... Porzio, L. (2022). Understanding coralline algal responses to ocean acidification: Meta-analysis and synthesis. *Global Change Biology*, *28*(2), 362–374.

DeVries, T. (2014). The oceanic anthropogenic CO_2 sink: Storage, air-sea fluxes, and transports over the industrial era. *Global Biogeochemical Cycles*, *28*(7), 631–647.

Dickson, A., & Millero, F. J. (1987). A comparison of the equilibrium constants for the dissociation of carbonic acid in seawater media. *Deep Sea Research Part A. Oceanographic Research Papers*, *34*(10), 1733–1743.

Dickson, A. G. (1993). The measurement of seawater pH. *Marine Chemistry*, *44*(2-4), 131–142.

Dlugokencky, E., Thoning, K., Lan, X., & Tans, P. (2021). *NOAA greenhouse gas reference from atmospheric carbon dioxide dry air mole fractions from the NOAA GML carbon cycle cooperative global air sampling network.*

Doney, S. C., Busch, D. S., Cooley, S. R., & Kroeker, K. J. (2020). The impacts of ocean acidification on marine ecosystems and reliant human communities. *Annual Review of Environment and Resources*, *45*, 83–112.

Doney, S. C., Fabry, V. J., Feely, R. A., & Kleypas, J. A. (2009). Ocean acidification: the other CO_2 problem. *Annual review of marine science*, *1*, 169–192.

Dore, J. E., Lukas, R., Sadler, D. W., Church, M. J., & Karl, D. M. (2009). Physical and biogeochemical modulation of ocean acidification in the central North Pacific. *Proceedings of the National Academy of Sciences*, *106*(30), 12235–12240.

Egleston, E. S., Sabine, C. L., & Morel, F. M. (2010). Revelle revisited: Buffer factors that quantify the response of ocean chemistry to changes in DIC and

alkalinity. *Global Biogeochemical Cycles*, *24*(1).

Fay, A., & McKinley, G. (2013). Global trends in surface ocean pCO_2 from in situ data. *Global Biogeochemical Cycles*, *27*(2), 541–557.

Fay, A. R., Gregor, L., Landschützer, P., McKinley, G. A., Gruber, N., Gehlen, M., ... others (2021). SeaFlux: harmonization of air–sea CO_2 fluxes from surface pCO_2 data products using a standardized approach. *Earth System Science Data*, *13*(10), 4693–4710.

Feely, R., Takahashi, T., Wanninkhof, R., McPhaden, M., Cosca, C., Sutherland, S., & Carr, M.-E. (2006). Decadal variability of the air-sea CO_2 fluxes in the equatorial Pacific Ocean. *Journal of Geophysical Research: Oceans*, *111*(C8).

Feely, R. A., Doney, S. C., & Cooley, S. R. (2009). Ocean acidification: Present conditions and future changes in a high-CO_2 world. *Oceanography*, *22*(4), 36–47.

Feely, R. A., Sabine, C. L., Lee, K., Berelson, W., Kleypas, J., Fabry, V. J., & Millero, F. J. (2004). Impact of anthropogenic CO_2 on the $CaCO_3$ system in the oceans. *Science*, *305*(5682), 362–366.

Figuerola, B., Hancock, A. M., Bax, N., Cummings, V. J., Downey, R., Griffiths, H. J., ... Stark, J. S. (2021). A review and meta-analysis of potential impacts of ocean acidification on marine calcifiers from the Southern Ocean. *Frontiers in Marine Science*, *8*, 24.

Friedlingstein, P., Jones, M. W., O'Sullivan, M., Andrew, R. M., Bakker, D. C., Hauck, J., ... others (2022). Global carbon budget 2021. *Earth System Science Data*, *14*(4), 1917–2005.

Friedrich, T., Timmermann, A., Abe-Ouchi, A., Bates, N., Chikamoto, M., Church, M., ... others (2012). Detecting regional anthropogenic trends in ocean acidification against natural variability. *Nature Climate Change*, *2*(3), 167–171.

Gloege, L., Yan, M., Zheng, T., & McKinley, G. A. (2022). Improved quantification of ocean carbon uptake by using machine learning to merge global models and pCO_2 data. *Journal of Advances in Modeling Earth Systems*, *14*(2), e2021MS002620.

Gregor, L., & Gruber, N. (2021). OceanSODA-ETHZ: a global gridded data set of the surface ocean carbonate system for seasonal to decadal studies of ocean acidification. *Earth System Science Data*, *13*(2), 777–808.

Gruber, N., Bakker, D. C., DeVries, T., Gregor, L., Hauck, J., Landschützer, P., ... Müller, J. D. (2023). Trends and variability in the ocean carbon sink. *Nature Reviews Earth & Environment*, 1–16.

Gruber, N., Bates, N. R., & Keeling, C. D. (2002, dec). Interannual variability in the North Atlantic carbon sink. *Science*, *298*(5602), 2374–2378. Retrieved from `http://www.ncbi.nlm.nih.gov/pubmed/12493911` doi: 10.1126/science.1077077

Gruber, N., Clement, D., Carter, B. R., Feely, R. A., Van Heuven, S., Hoppema, M., ... others (2019). The oceanic sink for anthropogenic CO_2 from 1994 to 2007. *Science*, *363*(6432), 1193–1199.

Gruber, N., Hauri, C., Lachkar, Z., Loher, D., Frölicher, T. L., & Plattner, G.-K. (2012). Rapid progression of ocean acidification in the California Current System. *Science*, *337*(6091), 220–223.

Hall-Spencer, J. M., & Harvey, B. P. (2019). Ocean acidification impacts on coastal ecosystem services due to habitat degradation. *Emerging Topics in Life Sciences*, *3*(2), 197–206.

Harvey, B. P., Kon, K., Agostini, S., Wada, S., & Hall-Spencer, J. M. (2021). Ocean acidification locks algal communities in a species-poor early successional stage. *Global Change Biology*, *27*(10), 2174–2187.

Hauck, J., Zeising, M., Le Quéré, C., Gruber, N., Bakker, D. C. E., Bopp, L., ... Séférian, R. (2020, oct). Consistency and Challenges in the Ocean Carbon Sink Estimate for the Global Carbon Budget. *Frontiers in Marine Science*, *7*(October), 1–33. Retrieved from `https://www.frontiersin.org/articles/`

10.3389/fmars.2020.571720/full doi: 10.3389/fmars.2020.571720

Hoegh-Guldberg, O., Mumby, P. J., Hooten, A. J., Steneck, R. S., Greenfield, P., Gomez, E., ... Hatziolos, M. E. (2007, 12). Coral reefs under rapid climate change and ocean acidification. *Science*, *318*, 1737-1742. Retrieved from https://www.science.org/doi/10.1126/science.1152509 doi: 10.1126/science.1152509

Humphreys, M. P., Gregor, L., Pierrot, D., van Heuven, S., Lewis, E. R., & Wallace, D. W. (2020). *PyCO2SYS: marine carbonate system calculations in Python.* Retrieved from https://doi.org/10.5281/zenodo.3967359{\#}.XzJOEdRZo2g.mendeley doi: 10.5281/ZENODO.3967359

Ishii, M., Rodgers, K. B., Inoue, H. Y., Toyama, K., Sasano, D., Kosugi, N., ... others (2020). Ocean acidification from below in the tropical pacific. *Global Biogeochemical Cycles*, *34*(8), e2019GB006368.

Jiang, L.-Q., Carter, B. R., Feely, R. A., Lauvset, S. K., & Olsen, A. (2019). Surface ocean pH and buffer capacity: past, present and future. *Scientific reports*, *9*(1), 1–11.

Johnson, G. C., & Lyman, J. M. (2020). Warming trends increasingly dominate global ocean. *Nature Climate Change*, *10*(8), 757–761. Retrieved from https://doi.org/10.1038/s41558-020-0822-0 doi: 10.1038/s41558-020-0822-0

Keller, K. M., Joos, F., & Raible, C. C. (2014). Time of emergence of trends in ocean biogeochemistry. *Biogeosciences*, *11*(13), 3647–3659.

Khatiwala, S., Tanhua, T., Mikaloff Fletcher, S., Gerber, M., Doney, S. C., Graven, H. D., ... others (2013). Global ocean storage of anthropogenic carbon. *Biogeosciences*, *10*(4), 2169–2191.

Kim, J.-Y., Kang, D.-J., Lee, T., & Kim, K.-R. (2014). Long-term trend of CO_2 and ocean acidification in the surface water of the Ulleung Basin, the East Japan Sea inferred from the underway observational data. *Biogeosciences*, *11*(9), 2443–2454.

Kroeker, K. J., Kordas, R. L., Crim, R., Hendriks, I. E., Ramajo, L., Singh, G. S., ... Gattuso, J.-P. (2013). Impacts of ocean acidification on marine organisms: quantifying sensitivities and interaction with warming. *Global change biology*, *19*(6), 1884–1896.

Kwiatkowski, L., Torres, O., Bopp, L., Aumont, O., Chamberlain, M., Christian, J. R., ... others (2020). Twenty-first century ocean warming, acidification, deoxygenation, and upper-ocean nutrient and primary production decline from CMIP6 model projections. *Biogeosciences*, *17*(13), 3439–3470.

Landschützer, P., Gruber, N., & Bakker, D. C. (2016). Decadal variations and trends of the global ocean carbon sink. *Global Biogeochemical Cycles*, *30*(10), 1396–1417.

Landschützer, P., Gruber, N., Bakker, D. C., & Schuster, U. (2014). Recent variability of the global ocean carbon sink. *Global Biogeochemical Cycles*, *28*(9), 927–949.

Landschützer, P., Gruber, N., Bakker, D. C., Stemmler, I., & Six, K. D. (2018). Strengthening seasonal marine CO_2 variations due to increasing atmospheric CO_2. *Nature Climate Change*, *8*(2), 146–150.

Lauvset, S. K., & Gruber, N. (2014). Long-term trends in surface ocean ph in the north atlantic. *Marine Chemistry*, *162*, 71–76.

Lauvset, S. K., Gruber, N., Landschützer, P., Olsen, A., & Tjiputra, J. (2015). Trends and drivers in global surface ocean pH over the past 3 decades. *Biogeosciences*, *12*(5), 1285–1298.

Leseurre, C., Monaco, C. L., Reverdin, G., Metzl, N., Fin, J., Mignon, C., & Benito, L. (2022). Trends and drivers of sea surface fCO_2 and pH changes observed in the Southern Indian Ocean over the last two decades (1998–2019). *Biogeosciences*, *19*, 2599–2625.

Lewis, E., Wallace, D., & Allison, L. J. (1998). *Program developed for CO_2 system calculations* (Tech. Rep.). Brookhaven National Laboratory, Department of Applied Science, Upton, NY, United States.

Lovenduski, N. S., Gruber, N., Doney, S. C., & Lima, I. D. (2007). Enhanced CO_2 outgassing in the Southern Ocean from a positive phase of the Southern Annular Mode. *Global Biogeochemical Cycles*, *21*(2).

Matsumoto, K., & Gruber, N. (2005). How accurate is the estimation of anthropogenic carbon in the ocean? an evaluation of the ΔC^* method. *Global Biogeochemical Cycles*, *19*(3).

McKinley, G. A., Follows, M. J., & Marshall, J. (2004). Mechanisms of air-sea CO_2 flux variability in the equatorial Pacific and the North Atlantic. *Global Biogeochemical Cycles*, *18*(2).

McNeil, B., & Matear, R. (2013). The non-steady state oceanic CO_2 signal: its importance, magnitude and a novel way to detect it. *Biogeosciences*, *10*(4), 2219–2228.

Mehrbach, C., Culberson, C., Hawley, J., & Pytkowicx, R. (1973). Measurement of the apparent dissociation constants of carbonic acid in seawater at atmospheric pressure 1. *Limnology and oceanography*, *18*(6), 897–907.

Mikaloff Fletcher, S. E., Gruber, N., Jacobson, A. R., Doney, S. C., Dutkiewicz, S., Gerber, M., ... others (2006). Inverse estimates of anthropogenic CO_2 uptake, transport, and storage by the ocean. *Global biogeochemical cycles*, *20*(2).

Mucci, A., et al. (1983). The solubility of calcite and aragonite in seawater at various salinities, temperatures, and one atmosphere total pressure. *American Journal of Science*, *283*(7), 780–799.

Olafsson, J., Olafsdottir, S., Benoit-Cattin, A., & Takahashi, T. (2010). The Irminger Sea and the Iceland Sea time series measurements of sea water carbon and nutrient chemistry 1983–2008. *Earth System Science Data*, *2*(1), 99–104.

Orr, J. C. (2011). Recent and future changes in ocean carbonate chemistry. *Ocean acidification*, *1*, 41–66.

Orr, J. C., Fabry, V. J., Aumont, O., Bopp, L., Doney, S. C., Feely, R. A., ... others (2005). Anthropogenic ocean acidification over the twenty-first century and its impact on calcifying organisms. *Nature*, *437*(7059), 681–686.

Radford, C., Collins, S., Munday, P., & Parsons, D. (2021). Ocean acidification effects on fish hearing. *Proceedings of the Royal Society B*, *288*(1946), 20202754.

Raimondi, L., Matthews, J. B. R., Atamanchuk, D., Azetsu-Scott, K., & Wallace, D. W. (2019). The internal consistency of the marine carbon dioxide system for high latitude shipboard and in situ monitoring. *Marine Chemistry*, *213*, 49–70.

Reynolds, R. W., Smith, T. M., Liu, C., Chelton, D. B., Casey, K. S., & Schlax, M. G. (2007). Daily high-resolution-blended analyses for sea surface temperature. *Journal of climate*, *20*(22), 5473–5496.

Rödenbeck, C., Bakker, D. C., Gruber, N., Iida, Y., Jacobson, A. R., Jones, S., ... others (2015). Data-based estimates of the ocean carbon sink variability–first results of the Surface Ocean pCO_2 Mapping intercomparison (SOCOM). *Biogeosciences*, *12*, 7251–7278.

Rodgers, K. B., Lin, J., & Frölicher, T. L. (2015). Emergence of multiple ocean ecosystem drivers in a large ensemble suite with an Earth system model. *Biogeosciences*, *12*(11), 3301–3320.

Sabine, C. L., Feely, R. A., Gruber, N., Key, R. M., Lee, K., Bullister, J. L., ... others (2004). The oceanic sink for anthropogenic CO_2. *Science*, *305*(5682), 367–371.

Sallée, J.-B., Pellichero, V., Akhoudas, C., Pauthenet, E., Vignes, L., Schmidtko, S., ... Kuusela, M. (2021). Summertime increases in upper-ocean stratification

and mixed-layer depth. *Nature*, *591*(7851), 592–598.

Sarmiento, J., & Gruber, N. (2006). *Ocean biogeochemical dynamics*. Princeton University Press.

Schlunegger, S., Rodgers, K. B., Sarmiento, J. L., Frölicher, T. L., Dunne, J. P., Ishii, M., & Slater, R. (2019). Emergence of anthropogenic signals in the ocean carbon cycle. *Nature climate change*, *9*(9), 719–725.

Sutton, A. J., Feely, R. A., Sabine, C. L., McPhaden, M. J., Takahashi, T., Chavez, F. P., ... Mathis, J. T. (2014). Natural variability and anthropogenic change in equatorial Pacific surface ocean pCO_2 and pH. *Global Biogeochemical Cycles*, *28*(2), 131–145.

Takahashi, T., Sutherland, S. C., Chipman, D. W., Goddard, J. G., Ho, C., Newberger, T., ... Munro, D. (2014). Climatological distributions of pH, pCO_2, total CO_2, alkalinity, and $CaCO_3$ saturation in the global surface ocean, and temporal changes at selected locations. *Marine Chemistry*, *164*, 95–125.

Terhaar, J., Frölicher, T. L., & Joos, F. (2023). Ocean acidification in emission-driven temperature stabilization scenarios: the role of TCRE and non-CO_2 greenhouse gases. *Environmental Research Letters*.

Tilbrook, B., Jewett, E. B., DeGrandpre, M. D., Hernandez-Ayon, J. M., Feely, R. A., Gledhill, D. K., ... others (2019). An enhanced ocean acidification observing network: from people to technology to data synthesis and information exchange. *Frontiers in Marine Science*, 337.

Tjiputra, J. F., Olsen, A., Bopp, L., Lenton, A., Pfeil, B., Roy, T., ... Heinze, C. (2014). Long-term surface pCO_2 trends from observations and models. *Tellus B: Chemical and Physical Meteorology*, *66*(1), 23083.

Weiss, R. (1974). Carbon dioxide in water and seawater: The solubility of non-ideal gas. *Marine Chemistry*, *2*, 203–215.

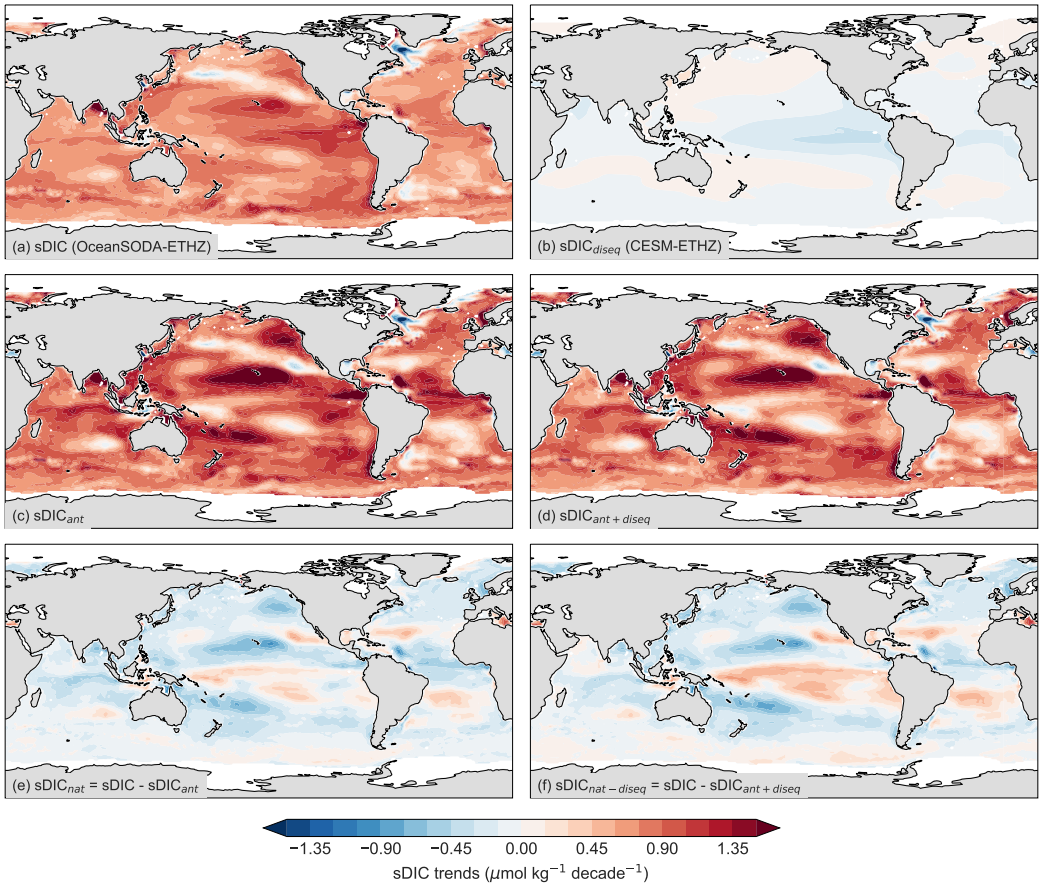

Figure S1. Maps of the slopes of salinity normalized DIC (sDIC) for various components. (a) sDIC trends from OceanSODA-ETHZ (Gregor & Gruber, 2021). (b) The disequilibrium term was calculated as the difference between oceanic and atmospheric pCO_2 for a CESM-ETHZ model run with increasing CO_2 and constant climate (run C). The pCO_2 disequilibrium was added to OceanSODA-ETHZ pCO_2 from which DIC was calculated with *PyCO2SYS*. (c) The expected increase in sDIC if pCO_2 followed atmospheric pCO_2 perfectly. (d) The increase in sDIC when accounting for the disequilibrium where uptake slows due to natural outgassing. (e) The slope of the natural sDIC component is calculated as the residual of (a) - (c). (f) The slope of the natural sDIC component including the disequilibrium term calculated as (a) - (d).

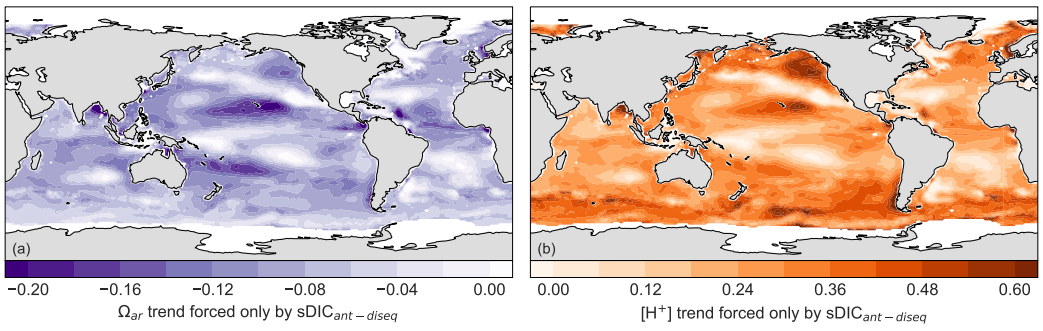

Figure S2. Expected increases in (a) Ω_{ar} and (b) [H^+] due to an increase in sDIC$_{ant+diseq}$ (shown in Figure S1d).

Table S1. Trends for pH and Ω_{ar} (units per decade) from various sources in the literature compared with OceanSODA-ETHZ for the same periods. Note that these trends may not compare well with OceanSODA-ETHZ results due to the different methods used to calculate the trends.

			pH (decade^{-1})		Ω_{ar} (decade^{-1})		
Station	Location	Period	Trend	Literature	Trend	Literature	Reference
BATS	32.0°N, 64.0°W	1983-2012	-0.014 ± 0.000	-0.017 ± 0.001	-0.066 ± 0.006	-0.095 ± 0.007	(Bates et al., 2014)
		1983-2020	-0.016 ± 0.000	-0.019 ± 0.001	-0.060 ± 0.004	-0.090 ± 0.010	(Bates & Johnson, 2020)
HOT	22.8°N, 158.0°W	1988-2007	-0.014 ± 0.001	-0.019 ± 0.002	-0.095 ± 0.013		(Dore et al., 2009)
		1988-2012	-0.015 ± 0.001	-0.016 ± 0.001	-0.098 ± 0.009	-0.084 ± 0.011	(Bates et al., 2014)
ESTOC	29.0°N, 15.5°W	1995-2012	-0.016 ± 0.001	-0.018 ± 0.002	-0.072 ± 0.014	-0.115 ± 0.023	(Bates et al., 2014)
Iceland Sea	68.0°N, 12.7°W	1983-2012	-0.019 ± 0.001	-0.014 ± 0.005	-0.056 ± 0.006	-0.018 ± 0.027	(Bates et al., 2014)
Irminger Sea	64.3°N, 28.0°W	1983-2012	-0.018 ± 0.000	-0.026 ± 0.006	-0.046 ± 0.007	-0.080 ± 0.040	(Bates et al., 2014)
Munida	45.7°S, 171.5°E	1998-2012	-0.019 ± 0.001	-0.013 ± 0.003	-0.122 ± 0.024	-0.085 ± 0.026	(Bates et al., 2014)
CARIACO	10.5°N, 64.7°W	1995-2012		-0.025 ± 0.004		-0.066 ± 0.028	(Bates et al., 2014)
137°E tropics	5-10°N, 137.0°E	1983-2017	-0.013 ± 0.000	-0.012 ± 0.008	-0.065 ± 0.005	-0.081 ± 0.050	(Ono et al., 2019)
137°E subtropics	20-22°N, 137.0°E	1983-2017	-0.016 ± 0.000	-0.017 ± 0.007	-0.080 ± 0.005	-0.113 ± 0.040	(Ono et al., 2019)
137°E Kuriosho	26-30°N, 137.0°E	1983-2017	-0.017 ± 0.001	-0.019 ± 0.008	-0.090 ± 0.006	-0.121 ± 0.050	(Ono et al., 2019)

Table S2. Comparison of trends (units per decade) for long-term observation stations. pH and Ω_{ar} were calculated from DIC and Alk for the observation stations and OceanSODA-ETHZ was calculated from pCO_2 and Alk. Uncertainties are the standard error associated with the slope coefficient and do not include other uncertainties associated with measurements or predictions.

			pH		Ω_{ar}	
Station	Location	Period	Observations	OS-ETHZ	Observations	OS-ETHZ
BATS	31.5°N, 64.5°W	1992-2021	-0.0166 ± 0.001	-0.0174 ± 0.000	-0.0625 ± 0.010	-0.0605 ± 0.005
HOT	22.5°N, 158.5°W	1989-2021	-0.0180 ± 0.001	-0.0182 ± 0.001	-0.0888 ± 0.006	-0.0826 ± 0.005
ESTOC	29.5°N, 15.5°W	1995-2009	-0.0139 ± 0.003	-0.0155 ± 0.001	-0.1375 ± 0.013	-0.0676 ± 0.020

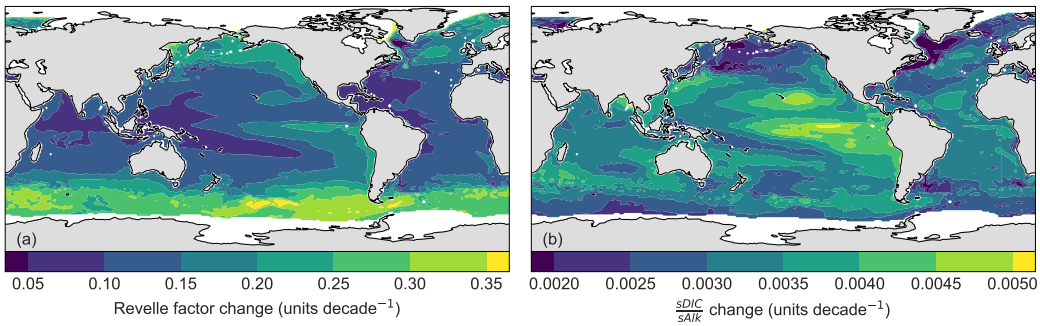

Figure S3. (a) Map showing the rates of Revelle factor change and (b) map showing the rates of DIC/Alk ratio change.

Table S3. Slopes of Ω_{ar} (units per decade) decomposed into mechanisms (Mech.) for each driver. The regions are biomes from (Fay & McKinley, 2014), where the ice-covered biomes are not presented. We decompose sDIC into anthropogenic ($sDIC^{ant}$) and natural ($sDIC^{nat}$) components, where the latter is the residual of sDIC minus the anthropogenic component. We also show the actual trend for the variable (Trend) and the sum of the decomposed components (Σ). The mechanisms are taken from Eq 2., where m.e. indicates the mass effect.

Region	Trend	Σ	Mech.	$sDIC^{ant}$	$sDIC^{nat}$	sDIC	sAlk	Temp	FW
GLOBAL	-0.0711	-0.0712	ΔX	-0.0869	0.0158	-0.0711	-0.0051	0.0028	0.0020
			ω_X	-0.0039	0.0005	-0.0034	0.0000	-0.0000	-0.0000
			Ω_{ar} m.e.	0.0044	-0.0006	0.0038	-0.0001	-0.0001	0.0000
NP-SPSS	-0.0479	-0.0491	ΔX	-0.0736	0.0269	-0.0467	-0.0054	0.0022	0.0005
			ω_X	-0.0025	0.0005	-0.0019	-0.0003	-0.0000	-0.0000
			Ω_{ar} m.e.	0.0032	-0.0008	0.0024	0.0002	-0.0001	-0.0000
NP-STSS	-0.0689	-0.0697	ΔX	-0.0844	0.0243	-0.0601	-0.0167	0.0040	0.0032
			ω_X	-0.0028	0.0006	-0.0022	-0.0012	-0.0000	-0.0000
			Ω_{ar} m.e.	0.0031	-0.0007	0.0024	0.0012	-0.0001	-0.0002
NP-STPS	-0.0809	-0.0818	ΔX	-0.1074	0.0272	-0.0801	-0.0055	0.0036	0.0003
			ω_X	-0.0033	0.0003	-0.0030	-0.0007	-0.0000	-0.0000
			Ω_{ar} m.e.	0.0035	-0.0004	0.0032	0.0007	-0.0001	-0.0002
PEQU-W	-0.0647	-0.0652	ΔX	-0.0740	0.0092	-0.0648	-0.0115	0.0045	0.0069
			ω_X	-0.0035	0.0006	-0.0029	0.0000	-0.0000	-0.0000
			Ω_{ar} m.e.	0.0033	-0.0006	0.0027	-0.0000	-0.0001	-0.0000
PEQU-E	-0.0981	-0.0975	ΔX	-0.1074	0.0019	-0.1055	0.0079	0.0012	-0.0024
			ω_X	-0.0038	-0.0035	-0.0073	-0.0002	0.0000	-0.0000
			Ω_{ar} m.e.	0.0045	0.0038	0.0083	0.0002	0.0004	-0.0001
SP-STPS	-0.0795	-0.0796	ΔX	-0.0978	0.0180	-0.0798	-0.0039	0.0026	0.0014
			ω_X	-0.0038	0.0003	-0.0035	-0.0002	-0.0000	-0.0000
			Ω_{ar} m.e.	0.0042	-0.0004	0.0038	0.0002	-0.0001	-0.0001
NA-SPSS	-0.0452	-0.0457	ΔX	-0.0635	0.0261	-0.0374	-0.0139	0.0032	0.0023
			ω_X	-0.0027	0.0008	-0.0019	-0.0002	-0.0000	-0.0000
			Ω_{ar} m.e.	0.0034	-0.0010	0.0024	-0.0001	-0.0001	-0.0000
NA-STSS	-0.065	-0.0652	ΔX	-0.0873	0.0229	-0.0644	-0.0078	0.0037	0.0035
			ω_X	-0.0033	0.0009	-0.0024	-0.0002	-0.0000	-0.0000
			Ω_{ar} m.e.	0.0034	-0.0009	0.0025	0.0002	-0.0002	-0.0001
NA-STPS	-0.0676	-0.0673	ΔX	-0.0842	0.0103	-0.0739	-0.0033	0.0044	0.0057
			ω_X	-0.0034	0.0007	-0.0027	0.0000	-0.0000	-0.0000
			Ω_{ar} m.e.	0.0034	-0.0007	0.0027	-0.0000	-0.0001	-0.0001
AEQU	-0.0774	-0.0783	ΔX	-0.1254	0.0393	-0.0862	0.0074	0.0039	-0.0036
			ω_X	-0.0055	0.0023	-0.0032	0.0006	-0.0000	-0.0000
			Ω_{ar} m.e.	0.0059	-0.0024	0.0034	-0.0007	-0.0002	0.0003
SA-STPS	-0.0719	-0.071	ΔX	-0.0621	-0.0018	-0.0640	-0.0172	0.0025	0.0076
			ω_X	-0.0049	0.0015	-0.0034	0.0003	-0.0000	0.0000
			Ω_{ar} m.e.	0.0049	-0.0015	0.0034	-0.0003	-0.0001	0.0002
IND-STPS	-0.0734	-0.0737	ΔX	-0.0940	0.0205	-0.0735	-0.0064	0.0035	0.0026
			ω_X	-0.0047	0.0013	-0.0033	0.0002	-0.0000	0.0000
			Ω_{ar} m.e.	0.0048	-0.0013	0.0034	-0.0002	-0.0001	0.0001
SO-STSS	-0.0667	-0.0664	ΔX	-0.0771	0.0155	-0.0616	-0.0095	0.0021	0.0021
			ω_X	-0.0047	0.0008	-0.0039	0.0004	-0.0000	-0.0000
			Ω_{ar} m.e.	0.0055	-0.0009	0.0046	-0.0006	-0.0001	0.0001
SO-SPSS	-0.0616	-0.0605	ΔX	-0.0707	0.0033	-0.0674	0.0058	0.0004	-0.0006
			ω_X	-0.0041	0.0002	-0.0040	0.0008	-0.0000	-0.0000
			Ω_{ar} m.e.	0.0058	-0.0002	0.0055	-0.0011	-0.0000	0.0001

Table S4. The same as Table S3 but for $[H^+]$ in nmol · kg^{-1} · decade^{-1}.

Region	Trend	Σ	Mech.	sDIC^{ant}	sDIC^{nat}	sDIC	sAlk	Temp	FW
GLOBAL	0.2502	0.2853	ΔX	0.2510	-0.0438	0.2073	0.0106	0.0381	0.0037
			β_X	0.0083	-0.0010	0.0073	-0.0003	-0.0000	-0.0000
			$[H^+]$ m.e.	0.0195	-0.0025	0.0170	-0.0003	0.0019	0.0000
NP-SPSS	0.2777	0.314	ΔX	0.3274	-0.1165	0.2109	0.0171	0.0561	0.0012
			β_X	0.0085	-0.0020	0.0066	0.0009	-0.0000	-0.0001
			$[H^+]$ m.e.	0.0201	-0.0045	0.0156	0.0021	0.0033	0.0003
NP-STSS	0.2575	0.3006	ΔX	0.2333	-0.0695	0.1638	0.0418	0.0601	0.0071
			β_X	0.0054	-0.0012	0.0042	0.0026	-0.0000	-0.0001
			$[H^+]$ m.e.	0.0130	-0.0026	0.0104	0.0061	0.0036	0.0010
NP-STPS	0.2392	0.274	ΔX	0.2543	-0.0634	0.1910	0.0135	0.0449	0.0011
			β_X	0.0050	-0.0004	0.0045	0.0013	-0.0000	-0.0001
			$[H^+]$ m.e.	0.0126	-0.0011	0.0115	0.0029	0.0026	0.0008
PEQU-W	0.2124	0.2477	ΔX	0.1673	-0.0208	0.1464	0.0217	0.0512	0.0114
			β_X	0.0049	-0.0008	0.0040	-0.0000	-0.0000	-0.0001
			$[H^+]$ m.e.	0.0145	-0.0026	0.0119	-0.0001	0.0012	0.0001
PEQU-E	0.2852	0.3278	ΔX	0.3000	-0.0031	0.2969	-0.0188	0.0159	-0.0055
			β_X	0.0080	0.0064	0.0144	0.0002	0.0000	-0.0000
			$[H^+]$ m.e.	0.0169	0.0144	0.0313	0.0006	-0.0076	0.0004
SP-STPS	0.2427	0.2744	ΔX	0.2540	-0.0460	0.2080	0.0063	0.0336	0.0021
			β_X	0.0070	-0.0006	0.0064	0.0002	-0.0000	-0.0000
			$[H^+]$ m.e.	0.0164	-0.0016	0.0148	0.0006	0.0021	0.0003
NA-SPSS	0.2604	0.2973	ΔX	0.2321	-0.0992	0.1329	0.0545	0.0738	0.0085
			β_X	0.0077	-0.0024	0.0053	0.0006	-0.0000	-0.0001
			$[H^+]$ m.e.	0.0185	-0.0064	0.0121	0.0030	0.0062	0.0005
NA-STSS	0.229	0.2634	ΔX	0.2281	-0.0602	0.1678	0.0172	0.0500	0.0067
			β_X	0.0059	-0.0016	0.0043	0.0005	-0.0000	-0.0000
			$[H^+]$ m.e.	0.0151	-0.0042	0.0109	0.0011	0.0045	0.0004
NA-STPS	0.2155	0.2488	ΔX	0.1870	-0.0229	0.1641	0.0064	0.0506	0.0095
			β_X	0.0048	-0.0009	0.0039	-0.0000	-0.0000	-0.0001
			$[H^+]$ m.e.	0.0137	-0.0025	0.0112	0.0000	0.0029	0.0003
AEQU	0.2187	0.2457	ΔX	0.2923	-0.0906	0.2017	-0.0143	0.0470	-0.0062
			β_X	0.0082	-0.0034	0.0048	-0.0010	-0.0000	-0.0000
			$[H^+]$ m.e.	0.0222	-0.0092	0.0129	-0.0021	0.0039	-0.0010
SA-STPS	0.2241	0.2563	ΔX	0.1496	0.0041	0.1537	0.0366	0.0316	0.0141
			β_X	0.0080	-0.0024	0.0056	-0.0006	-0.0000	0.0000
			$[H^+]$ m.e.	0.0199	-0.0060	0.0139	-0.0011	0.0030	-0.0005
IND-STPS	0.2208	0.2527	ΔX	0.2196	-0.0474	0.1723	0.0133	0.0426	0.0049
			β_X	0.0071	-0.0021	0.0051	-0.0003	-0.0000	0.0000
			$[H^+]$ m.e.	0.0191	-0.0055	0.0136	-0.0007	0.0023	-0.0004
SO-STSS	0.2654	0.303	ΔX	0.2559	-0.0500	0.2060	0.0244	0.0380	0.0050
			β_X	0.0119	-0.0019	0.0100	-0.0014	-0.0000	-0.0000
			$[H^+]$ m.e.	0.0258	-0.0041	0.0217	-0.0024	0.0021	-0.0004
SO-SPSS	0.325	0.3656	ΔX	0.3584	-0.0165	0.3419	-0.0256	0.0121	-0.0023
			β_X	0.0168	-0.0007	0.0160	-0.0031	-0.0000	-0.0000
			$[H^+]$ m.e.	0.0345	-0.0018	0.0327	-0.0058	0.0004	-0.0007

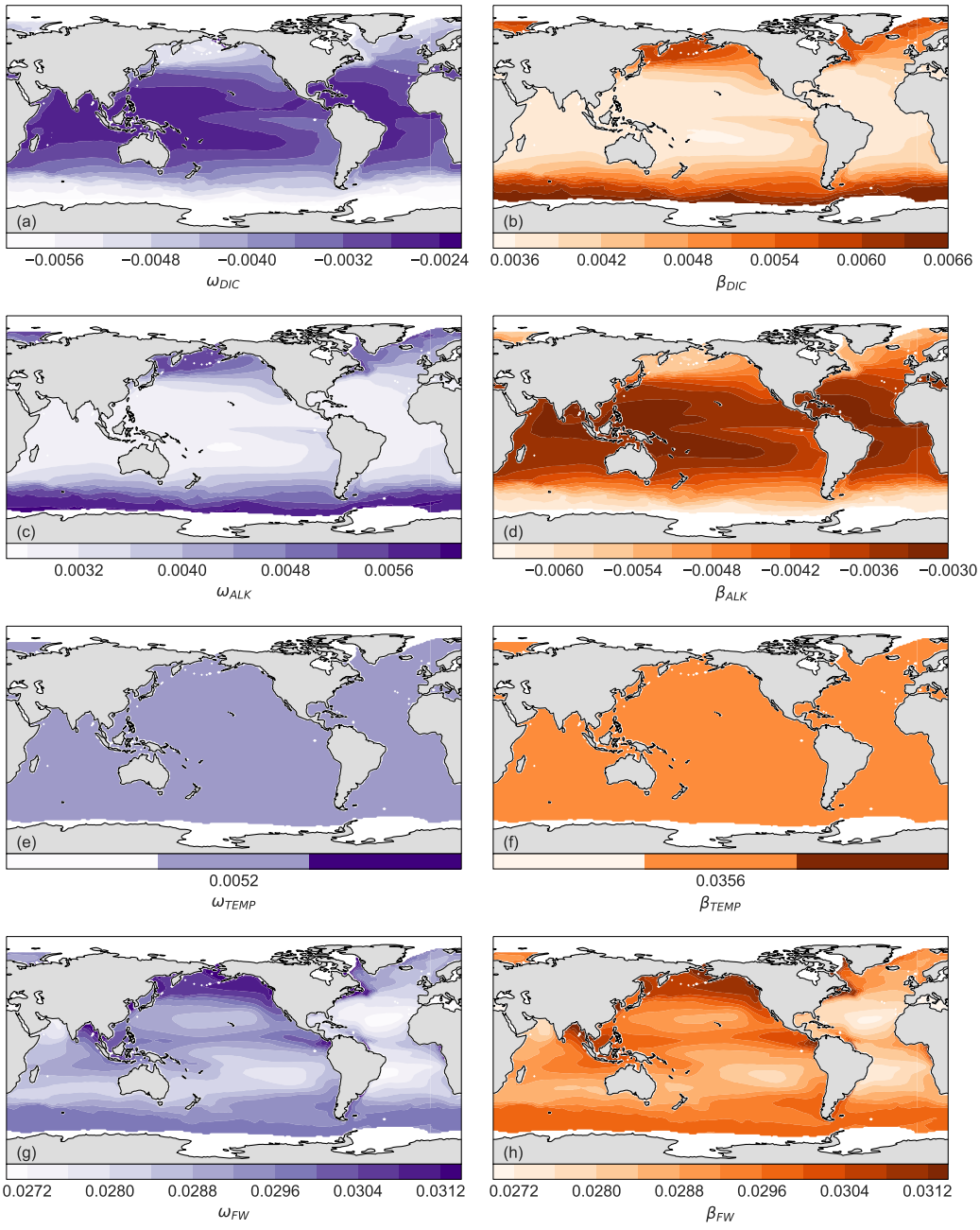

Figure S4. Maps depicting the average sensitivities of Ω (left) and $[H^+]$ (right) to changes in sDIC (a,b), sAlk (c,d), temperature (e,f), and freshwater input (g,h) in the period 1982-2020.

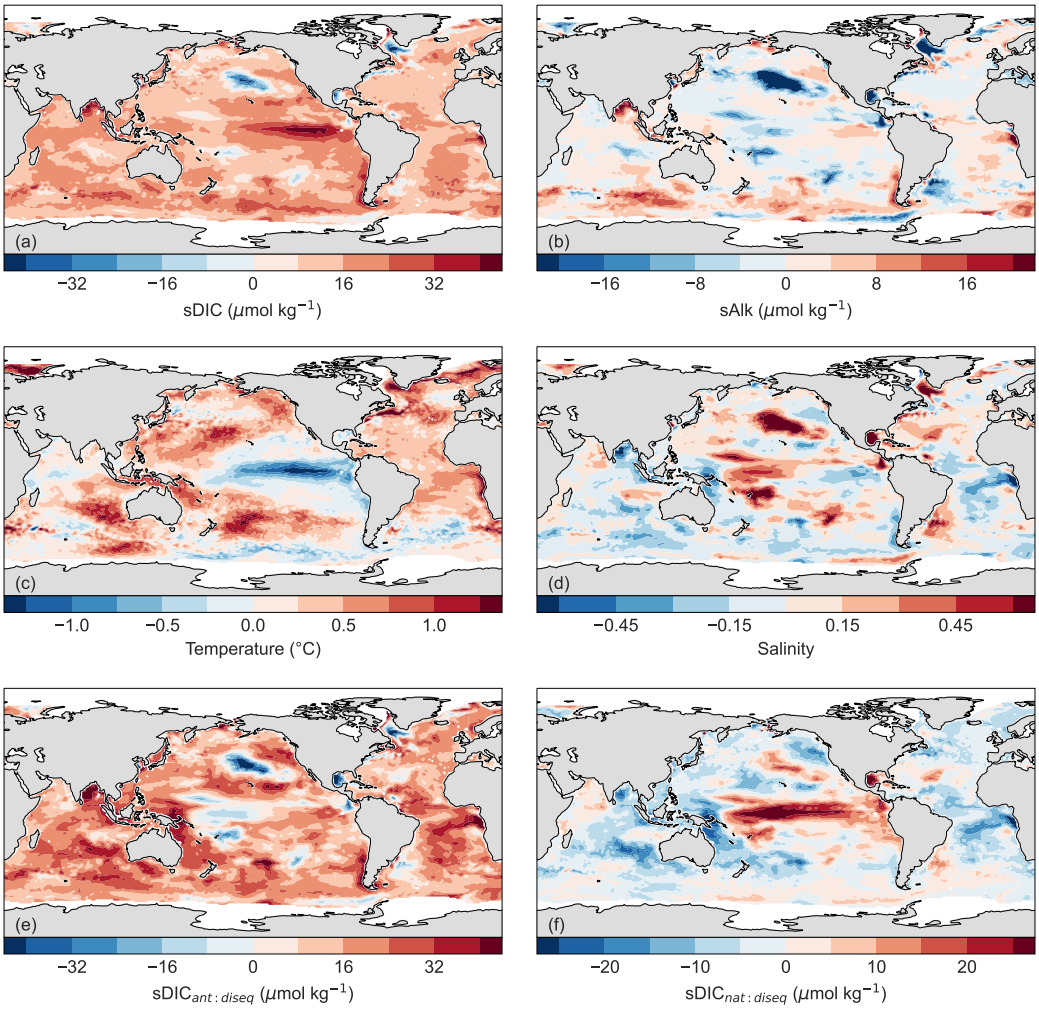

Figure S5. Maps showing the mean change (ΔX in Eq 2 and 3) in (a) sDIC, (b) sAlk, (c) temperature, (d) freshwater input, (e) $\text{sDIC}_{ant:diseq}$, and (f) $\text{sDIC}_{nat:diseq}$ from 1982 to 2021. Note that the mean change is calculated with $\Delta X = \sum_{i=1}^{N} (X_i - X_0)/N$ where X is the driver, i is the time step (years), X_0 is the first time step in X and N is the total number of years (40).

Table S5. Comparison of interannual variability among seven pCO2 products from the lowest to highest relative to OceanSODA-ETHZ: OceanSODA-ETHZ (Gregor & Gruber, 2021), CSIR-ML6 version 2019a (Gregor et al., 2019), CMEMS-FFNN (Denvil-Sommer et al., 2019), NIES-FNN (Zeng et al., 2015), MPI-SOMFFN (Landschützer et al., 2016), JMA-MLR (Iida et al., 2021), and Jena-MLS (Rödenbeck et al., 2013). Interannual variability in other data sets is scaled proportionally to that of OceanSODA-ETHZ, which is set to 1 by default.

Product	Scaled interannual variability
OceanSODA-ETHZ	1.00
CSIR-ML6 version 2019a	1.10
CMEMS-FFNN	1.31
NIES-FNN	1.56
MPI-SOMFFN	2.14
JMA-MLR	2.36
Jena-MLS	3.21

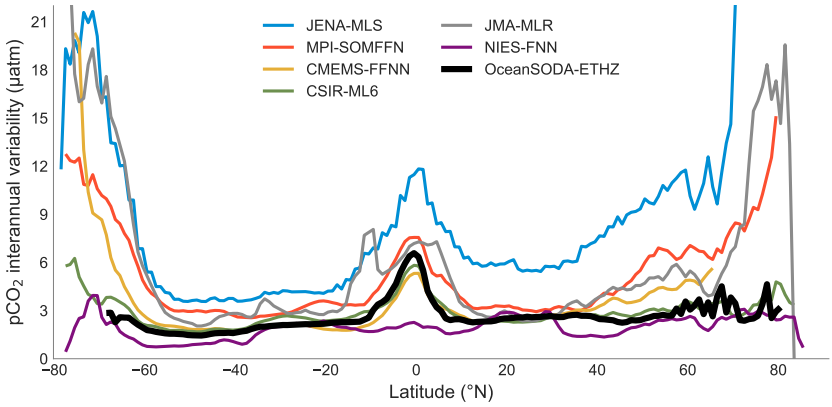

Figure S6. Comparison of zonally averaged interannual variability of pCO2 for the seven pCO2 products shown in Table S5.

References

Bates, N. R., Astor, Y. M., Church, M. J., Currie, K., Dore, J. E., González-Dávila, M., ... Santana-Casiano, J. M. (2014). A time-series view of changing surface ocean chemistry due to ocean uptake of anthropogenic CO_2 and ocean acidification. *Oceanography*, *27*(1), 126–141.

Bates, N. R., & Johnson, R. J. (2020). Acceleration of ocean warming, salinification, deoxygenation and acidification in the surface subtropical north atlantic ocean. *Communications Earth & Environment*, *1*(1), 33.

Denvil-Sommer, A., Gehlen, M., Vrac, M., & Mejia, C. (2019). Lsce-ffnn-v1: a two-step neural network model for the reconstruction of surface ocean pco 2 over the global ocean. *Geoscientific Model Development*, *12*(5), 2091–2105.

Dore, J. E., Lukas, R., Sadler, D. W., Church, M. J., & Karl, D. M. (2009). Physical and biogeochemical modulation of ocean acidification in the central North Pacific. *Proceedings of the National Academy of Sciences*, *106*(30), 12235–12240.

Fay, A., & McKinley, G. (2014). Global open-ocean biomes: mean and temporal variability. *Earth System Science Data*, *6*(2), 273–284.

Gregor, L., & Gruber, N. (2021). OceanSODA-ETHZ: a global gridded data set of the surface ocean carbonate system for seasonal to decadal studies of ocean acidification. *Earth System Science Data*, *13*(2), 777–808.

Gregor, L., Lebehot, A. D., Kok, S., & Scheel Monteiro, P. M. (2019). A comparative assessment of the uncertainties of global surface ocean CO_2 estimates using a machine-learning ensemble (CSIR-ML6 version 2019a)–have we hit the wall? *Geoscientific Model Development*, *12*(12), 5113–5136.

Iida, Y., Takatani, Y., Kojima, A., & Ishii, M. (2021). Global trends of ocean CO_2 sink and ocean acidification: an observation-based reconstruction of surface ocean inorganic carbon variables. *Journal of Oceanography*, *77*(2), 323–358.

Landschützer, P., Gruber, N., & Bakker, D. C. (2016). Decadal variations and trends of the global ocean carbon sink. *Global Biogeochemical Cycles*, *30*(10), 1396–1417.

Ono, H., Kosugi, N., Toyama, K., Tsujino, H., Kojima, A., Enyo, K., ... Ishii, M. (2019). Acceleration of Ocean Acidification in the Western North Pacific. *Geophysical Research Letters*, *46*(22), 13161–13169. doi: 10.1029/2019GL085121

Rödenbeck, C., Keeling, R. F., Bakker, D. C., Metzl, N., Olsen, A., Sabine, C., & Heimann, M. (2013). Global surface-ocean pCO_2 and sea–air CO_2 flux variability from an observation-driven ocean mixed-layer scheme. *Ocean Science*, *9*(2), 193–216.

Zeng, J., Nojiri, Y., Nakaoka, S.-i., Nakajima, H., & Shirai, T. (2015). Surface ocean CO_2 in 1990–2011 modelled using a feed-forward neural network. *Geoscience Data Journal*, *2*(1), 47–51.